JOURNAL OF GEOPHYSICAL RESEARCH, VOL. 112, D14307, doi:10.1029/2006JD008168, 2007

Impact of long-range correlations on trend detection in total ozone

Dmitry I. Vyushin,[1] Vitali E. Fioletov,[2] and Theodore G. Shepherd[1]

Received 19 October 2006; revised 9 March 2007; accepted 28 March 2007; published 24 July 2007.

[1] Total ozone trends are typically studied using linear regression models that assume a first-order autoregression of the residuals [so-called AR(1) models]. We consider total ozone time series over 60°S–60°N from 1979 to 2005 and show that most latitude bands exhibit long-range correlated (LRC) behavior, meaning that ozone autocorrelation functions decay by a power law rather than exponentially as in AR(1). At such latitudes the uncertainties of total ozone trends are greater than those obtained from AR(1) models and the expected time required to detect ozone recovery correspondingly longer. We find no evidence of LRC behavior in southern middle-and high-subpolar latitudes (45°–60°S), where the long-term ozone decline attributable to anthropogenic chlorine is the greatest. We thus confirm an earlier prediction based on an AR(1) analysis that this region (especially the highest latitudes, and especially the South Atlantic) is the optimal location for the detection of ozone recovery, with a statistically significant ozone increase attributable to chlorine likely to be detectable by the end of the next decade. In northern middle and high latitudes, on the other hand, there is clear evidence of LRC behavior. This increases the uncertainties on the long-term trend attributable to anthropogenic chlorine by about a factor of 1.5 and lengthens the expected time to detect ozone recovery by a similar amount (from ~2030 to ~2045). If the long-term changes in ozone are instead fit by a piecewise-linear trend rather than by stratospheric chlorine loading, then the strong decrease of northern middle- and high-latitude ozone during the first half of the 1990s and its subsequent increase in the second half of the 1990s projects more strongly on the trend and makes a smaller contribution to the noise. This both increases the trend and weakens the LRC behavior at these latitudes, to the extent that ozone recovery (according to this model, and in the sense of a statistically significant ozone increase) is already on the verge of being detected. The implications of this rather controversial interpretation are discussed.

Citation: Vyushin, D., V. E. Fioletov, and T. G. Shepherd (2007), Impact of long-range correlations on trend detection in total ozone, *J. Geophys. Res.*, *112*, D14307, doi:10.1029/2006JD008168.

1. Introduction

[2] The problem of the long-term decline of stratospheric ozone [e.g., *Stolarski et al.*, 1992; *World Meteorological Organization* (*WMO*), 1988] and, in recent years, of ozone recovery [e.g., *Newchurch et al.*, 2003; *Reinsel et al.*, 2005] has received wide attention from both the scientific community and the general public. Statistical models, particularly those based on multilinear regression methods, are commonly used for the detection of ozone changes [see *SPARC* (*Stratospheric Processes and Their Role in Climate*), 1998, and references therein]. Once a statistical model is established, it can be combined with other methods, for example, least squares, to find the best fit to the observations. Ozone variations are typically represented as a combination of a long-term trend, natural periodic components (seasonal cycle, solar cycle, quasi-biennial oscillation (QBO), etc.), and a random component (the residuals). Knowledge about autocorrelations of the residuals of the regression model is required for a correct estimation of the model parameter uncertainties. Since the earliest ozone assessments [e.g., *WMO*, 1988] it has been assumed that the residuals can be described by an AR(1) model, i.e., that the residual for a given month is proportional to the residual for the previous month plus random uncorrelated noise. In this case the autocorrelation function of the residuals $C(t)$ declines exponentially, i.e., $C(t) \sim \exp(-at)$, and the time series do not contain any significant long-term components other than those included explicitly in the model. Once the model parameters and their uncertainties have been estimated, they can be used, for example, to calculate the number of years required to detect a trend of a given magnitude at a given level of statistical significance [*Weatherhead et al.*, 1998, 2000; *Reinsel et al.*, 2002].

[1]Department of Physics, University of Toronto, Toronto, Ontario, Canada.
[2]Environment Canada, Toronto, Ontario, Canada.

0148-0227/07/2006JD008168$09.00

[3] Geophysical time series do not always follow the AR(1) model, however. They commonly exhibit long-range correlated (LRC) behavior, and their autocorrelation functions decay by a power law, i.e., $C(t) \sim |t|^{2H-2}$, where $0.5 < H < 1$. The parameter H is called the Hurst exponent after the British hydrologist H.E. Hurst, who first observed this phenomenon [*Hurst*, 1951]. Numerous studies published during the last decade or so have demonstrated LRC behavior in various meteorological parameters [e.g., *Bloomfield*, 1992; *Pelletier*, 1997; *Tsonis et al.*, 1999; *Stephenson et al.*, 2000]. All these studies report Hurst exponents for climate time series, estimated using different statistical methods, in the range between 0.5 and 1.0.

[4] There are also indications that ozone time series are not always well described by the AR(1) model. *Toumi et al.* [2001] considered daily total ozone records from three west European stations (Arosa, Lerwick, and Camborne) and calculated Hurst exponents for deseasonalized and detrended time series (assuming a linear trend). All three time series exhibited Hurst exponents of about 0.78. However, the authors did not remove the QBO- and solar-cycle-related components, which could affect the estimate of the Hurst exponent. *Varotsos and Kirk-Davidoff* [2006] considered total ozone time series for large spatially averaged areas, but also removed only the seasonal cycle and the linear trend. The estimates of the Hurst exponents were calculated using detrended fluctuation analysis (DFA) of the first order [*Kantelhardt et al.*, 2001]. The DFA filters out polynomial trends whose order is less than the order of the DFA applied. The Hurst exponents for tropical ozone estimated by *Varotsos and Kirk-Davidoff* [2006] were about 1.1, which implies an infinite variance, since, in this case, the integral of spectral density diverges. However, the presence of periodic signals such as the QBO and solar cycle tends to increase the DFA estimate of the Hurst exponent [*Jánosi and Müller*, 2005].

[5] In recent years it has been established that a sizable fraction of the long-term ozone changes over northern midlatitudes can be related to long-term changes in dynamical processes [e.g., *Weiss et al.*, 2001; *Randel et al.*, 2002; *Hadjinicolaou et al.*, 2005]. Estimation of ozone trends requires a proper accounting for the effects of these processes on ozone. One approach is to add more terms to the statistical models used for trend calculations [e.g., *Reinsel et al.*, 2005; *Dhomse et al.*, 2006]. However, the physical mechanisms behind these dynamical effects on ozone are often not well understood, and therefore it is difficult to account for them properly in a statistical model (see further discussion in section 3.1). Furthermore, such nonperiodic components cannot be predicted, and thus such models cannot be used to estimate future behavior. An alternative approach is to consider the contribution of dynamical processes to ozone fluctuations to be part of the noise. In this case, the noise may be LRC and a proper estimation of the residuals' autocovariance is required.

[6] In this study we investigate the possible existence of LRC behavior in total ozone time series and study its effects on ozone trend significance estimates and on the number of years required for trend detection. We employ spectral methods of Hurst exponent estimation instead of DFA because they have a better mathematical foundation. The plan of the paper is as follows. The total ozone data used in the analysis are described in section 2. Section 3 is devoted to the statistical models and their estimates of the noise. We review the theoretical background in section 3.1. Long-term trends in total ozone are represented in terms of either the equivalent effective stratospheric chlorine (EESC) time series or a piecewise-linear trend (PWLT) with a turning point in early 1996. Evidence of LRC behavior in several total ozone time series, including station data, is given in section 3.2, while LRC behavior in TOMS (Total Ozone Mapping Spectrometer)/SBUV (Solar Backscatter Ultraviolet) zonal averages is quantified in section 3.3 and compared with AR(1) behavior. The significance of the long-term ozone decline is compared under two different assumptions for the ozone residuals [AR(1) versus LRC] in section 4.1. The recent positive ozone trend and the number of years required to detect this trend under the two different assumptions are compared in section 4.2 for both the EESC- and PWLT-derived trends. Some results for TOMS/SBUV-gridded total ozone data, showing longitudinal structure, are discussed in section 5. The main results are summarized and their implications discussed in section 6. An introduction to the theory of LRC processes is given in Appendix A. Some details of the spectral methods for Hurst exponent estimation are presented in Appendix B. Formulas elucidating the implications of LRC behavior for trend uncertainties and for the number of years to detect linear trends are derived in Appendix C.

2. Data

[7] The merged satellite data set used here is prepared by NASA and combines version 8 of TOMS and SBUV total ozone data [*Frith et al.*, 2004; *Stolarski and Frith*, 2006]; it is available from http://hyperion.gsfc.nasa.gov/Data_services/merged/mod_data.public.html. The data set provides a nearly continuous time series of zonal and gridded (10° latitude by 30° longitude grid) monthly mean total ozone values between 60°S and 60°N (higher latitudes have data gaps during polar night) for the period from November 1978 to December 2005. In our study we considered only the period from January 1979 to December 2005. Some data, particularly the data for August–September 1995 and May–June 1996, were missing. Zonal averages estimated from ground-based total ozone measurements [*Fioletov et al.*, 2002] were used to fill the gaps. In addition, Dobson monthly mean total ozone values from three sites (Mauna Loa, Buenos Aires, and Hohenpeissenberg) were also analyzed here. These data are available from the WMO World Ozone and UV Radiation Data Centre (http://www.woudc.org).

3. Analysis of Long-Range Correlations in Total Ozone Time Series

3.1. Statistical Methods

[8] A typical statistical model describing observations of monthly mean total ozone can be expressed in the form

$$\Omega(t) = a_0 + A(t) + Q(t) + S(t) + T(t) + X(t), \qquad (1)$$

where $\Omega(t)$ denotes total ozone, t is the number of months after the initial time (taken here as January 1979), a_0 is the mean, $A(t)$ represents the seasonal cycle, $Q(t)$ the quasi-biennial oscillation (QBO), $S(t)$ the solar cycle, $T(t)$ the

long-term trend, and $X(t)$ are the residuals (noise). We used $A(t) = \sum_{j=1}^{4} a_{2j-1}\sin(2\pi j\ t/12) + a_{2j}\cos(2\pi j\ t/12)$, $Q(t) = (a_9 + a_{10}\sin(2\pi t/12) + a_{11}\cos(2\pi\ t/12))w_{30}(t) + (a_{12} + a_{13}\sin(2\pi\ t/12) + a_{14}\cos(2\pi\ t/12))w_{50}(t)$, and $S(t) = (a_{15} + a_{16}\sin(2\pi\ t/12) + a_{17}\cos(2\pi\ t/12))S_{107}(t)$, where $w_{30}(t)$ and $w_{50}(t)$ are the equatorial zonally averaged zonal winds at 30 and 50 hPa, respectively (http://www.cpc.ncep.noaa.gov/data/indices/), and $S_{107}(t)$ is the solar flux at 10.7 cm (http://www.drao-ofr.hia-iha.nrc-cnrc.gc.ca/icarus/www/sol_home.shtml). We use winds at both 30 and 50 hPa, because they are about 90° out of phase, which allows a better representation of the QBO signal in total ozone. The $\sin(2\pi\ t/12)$ and $\cos(2\pi\ t/12)$ terms in $Q(t)$ and $S(t)$ represent seasonal dependence. To describe the long-term trend in total ozone, two commonly used approaches are the equivalent effective stratospheric chlorine time series, EESC(t) (http://fmiarc.fmi.fi/candidoz/proxies.html) [*Guillas et al.*, 2004; *Newman et al.*, 2004; *Fioletov and Shepherd*, 2005; *Stolarski et al.*, 2006; *Weatherhead and Andersen*, 2006] and a piecewise-linear trend with a turning point that is typically chosen in the second half of the 1990s. Similar to *Reinsel et al.* [2005] and *Miller et al.* [2006] we choose a turning point n_0 in January 1996, because of the changes in ozone behavior and in the EESC tendency in the late 1990s. Therefore we use either $T(t) = (a_{18} + a_{19}\sin(2\pi\ t/12) + a_{20}\cos(2\pi\ t/12))\mathrm{EESC}(t)$ or $T(t) = a_{18}T_1(t) + a_{19}T_2(t)$, where $T_1(t) = t$, for $0 < t \le n$, where n is the time series length (324 in our case), and

$$T_2(t) = \begin{cases} 0, & 0 < t \le n_0, \\ t - n_0, & n_0 < t \le n. \end{cases} \tag{2}$$

[9] In order to provide analytical expressions for trends and their uncertainties, we use relatively simple trend models similar to those used by *Reinsel et al.* [2002] and *Reinsel et al.* [2005]. In addition, one of the key principles of statistical modeling is that the model be parsimonious, namely, that it involve a minimum number of free parameters [*von Storch and Zwiers*, 1999]. The more parameters are introduced, the easier it is to fit the time series and there is a risk that an improved fit may be fortuitous. This is particularly critical when the time series are very limited, as is the case with total ozone. In this study, we therefore restrict ourselves to equation (1) and do not, for example, introduce 12 coefficients for each component in equation (1) to more fully account for seasonal dependences. We have checked that using 12 coefficients for the QBO and/or trend terms does not alter the statistical properties of the residuals.

[10] To test the impact of the El Chichon and Mt. Pinatubo volcanic eruptions we included SAGE aerosol optical depth observations into our regression model. For each eruption, the aerosol loading was added to the model with the time lag that maximized the correlation between total ozone residuals and the aerosols. It was found that inclusion of volcanic aerosols only slightly decreases the Hurst exponent north of 30°S. Qualitatively, the Hurst exponent distribution and other results stay the same.

[11] There are several reasons why we included the solar cycle and QBO into equation (1) but not other explanatory variables, for example, EP flux or tropopause height [see also *WMO*, 1998]. First, ozone changes could affect temperature and other dynamical variables. Clearly, the solar cycle is not affected by ozone. In addition, QBO and solar variations are reasonably well-explained variations; EP-flux-forcing variations are not, they are part of the climate noise. If LRC manifest themselves through the EP flux forcing and we remove this forcing, then we just transfer the problem to that of understanding LRC in EP flux forcing. Furthermore, the correlation between ozone and dynamical variables could be different at different spectral intervals. The ozone-temperature correlation is a good example: The two fields are positively correlated on daily and monthly timescales but negatively correlated on an annual basis during major volcanic eruptions [*Randel and Cobb*, 1994]. So the relationship between ozone and such variables cannot be described by a single regression coefficient. This is not an issue for QBO and solar forcing because the variability of the QBO and the solar signal is located in a narrow spectral range. The QBO and solar cycles create maxima in the ozone time series power spectrum that could affect LRC estimates [*Jánosi and Müller*, 2005]. Since we also want to estimate the number of years that is required to detect future changes, we have to make some assumptions about the statistical model terms. We cannot predict the future solar and QBO signals, but we know their power spectra. So their impact on the future trend errors can be estimated. It is hard to make any predictions of dynamical variables or even about their spectral characteristics.

[12] The parameters a_j of the model (1) are unknown coefficients identified by multilinear regression on the total ozone observations using least squares. The autocovariance of the residuals $X(t)$ affects the variance of a_j and should be properly accounted for. Certain assumptions are typically made about the behavior of $X(t)$. For example, the AR(1) model assumes that $X(t) = \phi X(t-1) + \varepsilon(t)$, where $\varepsilon(t)$ are independent, normally distributed random errors. Similarly, the AR(k) model assumes that $X(t) = \phi_1 X(t-1) + \ldots + \phi_k X(t-k) + \varepsilon(t)$. The parameter ϕ can be estimated after the estimation of the parameters a_j as the lag-one autocorrelation coefficient of the residuals, or it can be included in the model (1) directly and estimated simultaneously with the parameters a_j. In this study we follow the first approach, i.e., sequential estimation.

[13] A different methodology is used if the autocorrelation function of $X(t)$ decays by a power law, i.e., $C(t) \sim |t|^{2H-2}$, where $0.5 < H < 1$. The methods we use here are based on the fact that long-range correlations (dependence) in the time domain translate into a particular behavior of the spectral density around the origin. It follows from the Abelian theorem that, if the autocovariance $\gamma(t) \sim |t|^{2H-2}$ as $t \to \infty$, where $0.5 < H < 1$, the spectral density $f(\lambda) \sim b|\lambda|^{1-2H}$ as $\lambda \to 0$ [see *Taqqu*, 2002], where, by definition,

$$f(\lambda) = \frac{1}{2\pi} \sum_{t=-\infty}^{\infty} \gamma(t) e^{-it\lambda}.$$

In particular, the log of the spectral density is a linear function of $\log(\lambda)$ as $\lambda \to 0$. In contrast, the spectral density of an AR(1) process is a constant function of λ under the same conditions and can be considered as a particular case of a more general power law model. Thus, as shown in Appendix C, the results we obtain for the LRC model are generalizations of those for the AR(1) model and reduce to the latter when H tends to 0.5.

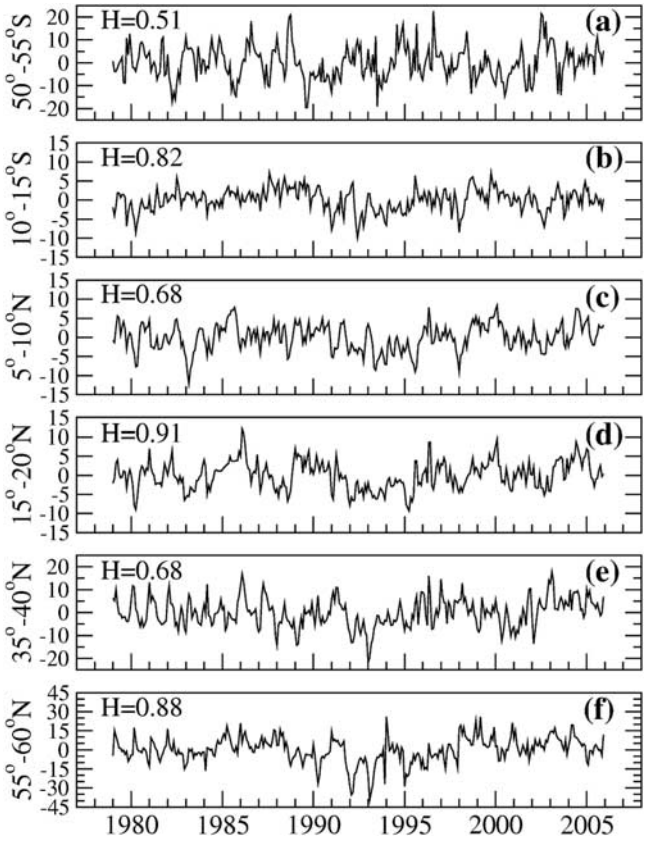

Figure 1. Monthly and zonal mean total ozone residuals in Dobson units obtained by filtering out the seasonal cycle, QBO, solar cycle, and EESC fit for various 5° latitude bands, as indicated. The Hurst exponent for each time series is indicated in the top left corner of each panel. Note the differences in the extent of low-frequency behavior in the time series with different Hurst exponents.

[14] The Geweke-Porter-Hudak estimator (GPHE) and the Gaussian semiparametric estimator (GSPE) are the two methods used in this study to estimate the two parameters, b and H, of the spectral density approximation, as described in Appendix B. GPHE estimates b and H by means of a linear regression of the log(periodogram) on log(λ). GSPE is a maximum likelihood estimator. The variances of the coefficients a_j of the statistical model (1) can be expressed as a function of b and H, as discussed in Appendix C. Furthermore, they can be used to estimate the number of years that is required to detect a statistically significant trend of a given magnitude (see Appendix C).

[15] The integral of the autocorrelation function from negative infinity to positive infinity, which is one way of quantifying a decorrelation time, is finite for an AR process and infinite for an LRC process. This means that, in contrast to the case with an AR process where the limit $t \gg t_{\text{decorrelation}}$ is well defined, two observations of an LRC process do not become statistically independent in the limit of arbitrarily large time separations [*von Storch and Zwiers*, 1999]. There are at least two possible physical origins of LRC behavior. One is based on the aggregation of an infinite number of AR(1) processes whose timescales satisfy certain conditions [*Granger*, 1980]. In practice, apparent LRC behavior may obtain from the aggregation of a finite number of AR(1) processes whose longest timescale is comparable to the length of the time series [*Maraun et al.*, 2004]. This is a definite possibility in the case of ozone time series where the records are comparatively short. A second possible origin of LRC behavior is a sequence of shocks or pulses with stochastic magnitudes and durations [*Parke*, 1999]. Volcanic eruptions could play such a role, although, as noted earlier, a direct link between aerosol loading and total ozone for the time period 1979–2005 does not appear to be associated with LRC behavior. The attribution of LRC behavior in total ozone is a separate topic which is not addressed here.

3.2. Illustrations of Long-Range Correlations

[16] Figure 1 shows time series of the residuals $X(t)$ for (1), obtained by filtering out the mean, seasonal cycle, QBO, solar flux, and EESC trend, for zonal and monthly mean total ozone in various latitude bands from 1979 to 2005. The corresponding Hurst exponents H, estimated using the Gaussian semiparametric estimator (GSPE), are also indicated. The latitude bands correspond to local maxima or minima of H (see Figure 4b below) and have been chosen to illustrate the different temporal behavior that is exemplified by large or small values of H. The time series with larger values of H tend to exhibit greater low-frequency variability with more instances of strong apparent "trends" over decadal timescales. Values of H that are close to 0.5 correspond to behavior that is not significantly different from AR(1), while the larger values of H are clear indicators of LRC behavior.

[17] To illustrate how the Hurst exponent is calculated by the Geweke-Porter-Hudak estimator we show power spectra of monthly mean total ozone residuals for three ground-based stations, Mauna Loa (19.5°N, 155.6°W), Buenos Aires (34.6°S, 58.5°W), and Hohenpeissenberg (47.8°N, 11.0°E), as well as for the corresponding nearest grid points and zonal averages from the merged satellite data set. For the purpose of comparison the period was limited to 1979–2005 for all data sets. Several months with missing data were filled by linear interpolation in time. Figure 2 shows the periodograms in log-log coordinates of the total ozone residuals for station data (Figures 2a, 2b, and 2c), for the nearest grid points from the merged data set (Figures 2d, 2e, and 2f), and for the corresponding zonal averages from the merged data set (Figures 2g, 2h, and 2i). The periodograms show an increase in variability with a decrease of frequency, which, as noted earlier, is a manifestation of LRC behavior. The solid straight lines are the best linear fits of the periodogram in log-log coordinates, corresponding to power law approximations in ordinary coordinates for the frequency bandwidth 1–27 years. The dashed straight lines represent the one sigma uncertainty envelope defined by the standard errors for slope and intercept. The linear fit of the periodogram represents the calculation of the Hurst exponent using the Geweke-Porter-Hudak estimator (GPHE, see Appendix B for details). Apart from Figures 2e, all slopes are statistically significantly less than zero, meaning that H is statistically significantly greater than 0.5 (H = (1 − slope)/2). Therefore eight out of the nine power spectra

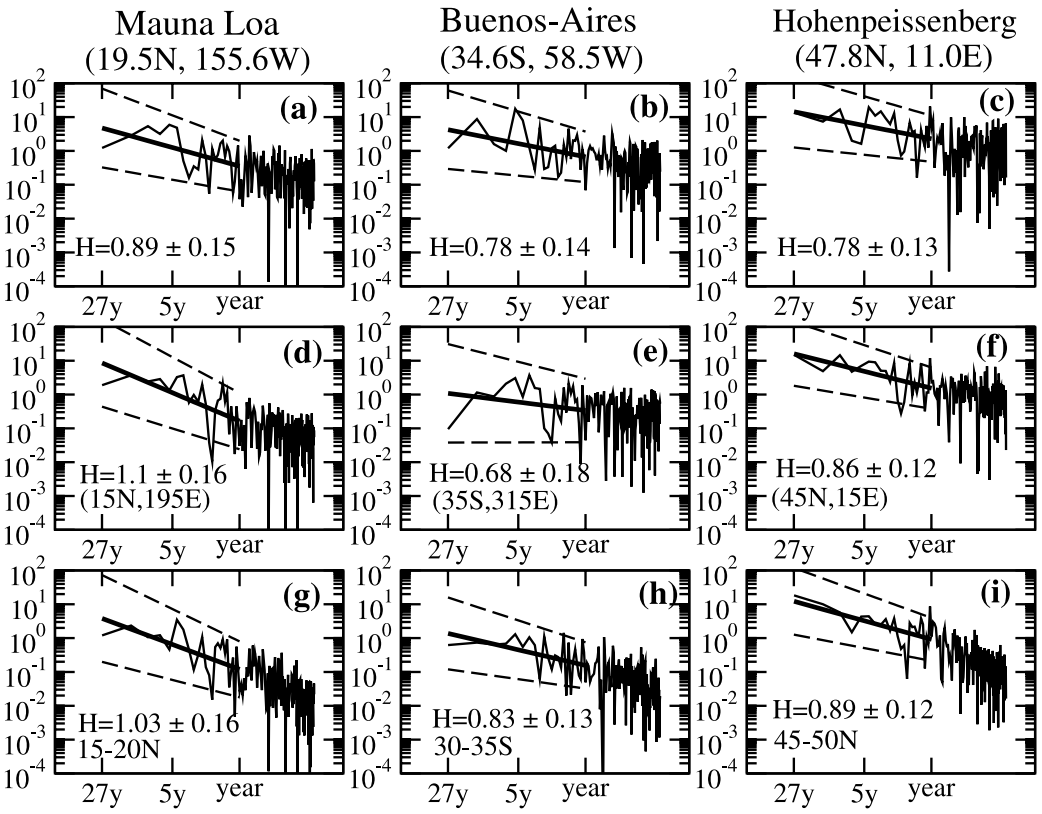

Figure 2. The periodograms in log-log coordinates for monthly mean total ozone residuals obtained by filtering out the seasonal cycle, QBO, solar flux, and EESC fit. The solid lines are the best linear fits, while the dashed lines represent the one sigma uncertainty envelope. (a, b, and c) Ground-based station data as indicated, (d, e, and f) the merged satellite data from the grid point nearest to the corresponding station, and (g, h, and i) the corresponding zonal averages from the merged satellite data.

shown reveal that the corresponding total ozone residuals are LRC (and the slopes for Figures 2b and 2e, which should be comparable, agree within the error bars). The zonal average time series typically have slightly greater Hurst exponents than the grid point time series from the same latitudinal belt since the average of several time series tends to have a Hurst exponent equal to the maximum of the Hurst exponents of the individual time series [*Granger*, 1980]. Additional evidence that this is the case for total ozone will be provided in section 5.

[18] To illustrate why it can be important to allow for LRC behavior in a statistical model, Figure 3a shows the autocorrelation function of the residuals $X(t)$ for 50°–55°N as well as the fits produced by various statistical models. In this case, H is significantly different from 0.5. Figure 3a shows that the AR(1) model (the short dashed curve) does not fit well the autocorrelation function of the total ozone residuals (the solid circles) for periods longer than several months. Even using higher order AR models such as AR(3) (the long dashed curve) does not improve the fit. The most parsimonious approximation of the solid circles is a simple power law function $a|t|^{2H-2}$ (the solid curve). Autocorrelation functions of the AR(1) and AR(3) models rapidly decay, while the power law function decays slowly and follows the autocorrelation function of the original time series.

[19] However, as seen in Figure 1, there are latitude bands where LRC behavior is not evident. For example, over 50°–55°S, where H is not significantly different from 0.5 (see the appropriate panel of Figure 1), the power law function does not provide a superior fit to the autocorrelation function of the total ozone residuals, whereas a reasonably good fit is provided by the AR(3) model (Figure 3b). Thus it is important to establish where LRC behavior is evident and where it is not.

3.3. Quantification of Long-Range Correlations in Zonally Averaged Ozone

[20] Ozone trend studies are typically performed using zonally averaged data. Part of the motivation for this lies in the approximate zonal symmetry of the stratosphere and thus of quantities such as ozone trends. By taking a zonal average of the data, longitudinal fluctuations (eddies) are removed, thereby reducing the standard deviation (noise level) of the time series while keeping the zonally symmetric trend unchanged. Thus zonal averaging usually leads to an increase of the signal-to-noise ratio. However, a drawback of zonal averaging is an increase in the strength of serial correlations.

[21] In this subsection we systematically analyze the zonally averaged total ozone residuals in the merged satellite data set as a function of latitude. What is considered a

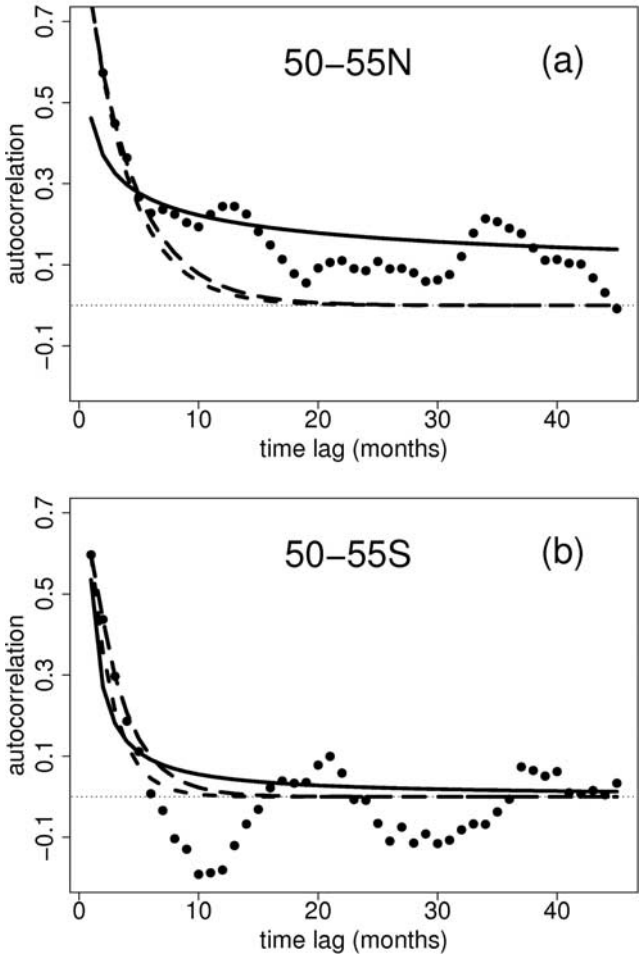

Figure 3. Autocorrelation function for two sample latitude bands (solid circles) of monthly and zonal mean total ozone residuals obtained by filtering out the seasonal cycle, QBO, solar flux, and EESC fit, together with that of various approximations (lines). The autocorrelation function of the best fit AR(1) model is shown by the short dashed curve, that of the AR(3) model by the long dashed curve, and that of the best fit power law function by the solid curve. The 50°–55°N latitude band (Figure 3a) shows clear evidence of LRC, while the 50°–55°S latitude band (Figure 3b) shows no such evidence.

residual depends on how the trend contribution is defined. We thus consider (and compare) the following two versions of the residuals, which represent the trend contribution in different ways: one with the EESC function and the other with the PWLT. The residuals are then analyzed using the AR(1), GPHE, and GSPE approaches. The GPHE and GSPE were applied to the frequency bandwidth from 1 to 27 years. The estimates for the square root of b and H for the case where the EESC trend is removed are shown in Figures 4a and 4b, respectively. The GPHE and GSPE provide consistent estimates for the Hurst exponents, although GPHE is more spatially noisy. All but one Hurst exponent shown in Figure 4b is less than one, i.e., the corresponding time series are second order stationary with finite and time-independent mean and standard deviation. The estimates of σ (standard deviation of the residuals) and ϕ (lag-one autocorrelation of the residuals) for the AR(1) model are also shown in Figure 4. Although $\sqrt{b}$ and σ, as well as H and ϕ, cannot be compared directly, they represent similar quantities as follows: the first pair is a measure of the variability of the residuals, while the second pair is an indicator of the persistence in the time series. It is interesting to note that the maxima and minima of b and σ, as well as of H and ϕ, tend to occur in roughly the same latitude bands.

[22] The theory for the distributions of H estimated by GPHE and GSPE exists only for the asymptotic case $m \rightarrow \infty$, where m is the number of frequencies used, with some other additional conditions [see *Robinson*, 1995a, 1995b]. Under these conditions the theorems proved by Robinson state that the estimates of H obtained by GPHE and GSPE are distributed normally with a mean equal to the true value of H and variances equal to $\pi^2/24m$ and $1/4m$, respectively. Therefore GSPE has a smaller asymptotic variance than

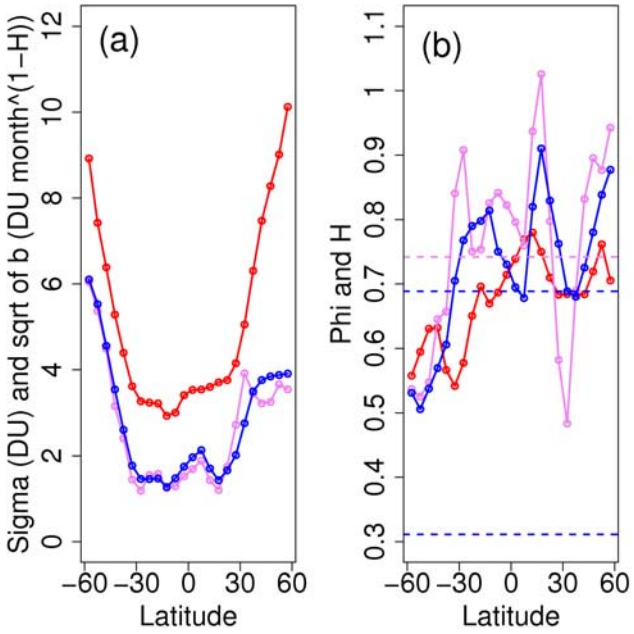

Figure 4. Estimates of various statistical parameters for monthly and zonal mean total ozone residuals obtained by filtering out the seasonal cycle, QBO, solar flux, and EESC fit, shown as functions of latitude. (a) Standard deviation σ calculated by AR(1) (red circles) and the square root of the parameter b calculated by GPHE (violet circles) and GSPE (blue circles) applied to the frequency bandwidth 1–27 years. (b) Month-to-month lag-one autocorrelation ϕ calculated by AR(1) (red circles) and the Hurst exponents calculated by GPHE (violet circles) and GSPE (blue circles). The violet (blue) dashed lines in Figure 4b indicate the 95% confidence intervals for GPHE (GSPE). Note that the lower 95% limit for GPHE is outside the figure frame. Thus time series for which the Hurst exponents lie above the dashed lines may be considered as LRC at the 95% significance level.

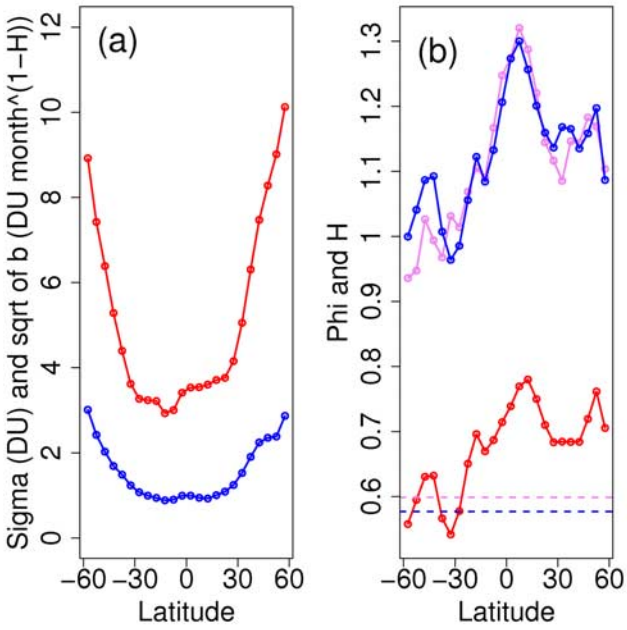

Figure 5. Same as Figure 4, but with GPHE and GSPE applied to the frequency bandwidth 2 months to 27 years. Note the different vertical scale in Figure 5b compared with Figure 4b. This analysis yields spurious results, namely, Hurst exponents greater than unity (indicating nonstationary behavior). The figure is included to highlight the importance of choosing an appropriate bandwidth (see text for further discussion).

GPHE by a factor of $\pi^2/6$. The values $0.5 \pm 1.96\ \pi/\sqrt{24m}$ and $0.5 \pm 1.96/(2\ \sqrt{m})$ are indicated in Figure 4b by dashed violet and blue lines, respectively. All Hurst exponent estimates located above these lines may be considered as greater than 0.5 with 95% statistical significance, meaning that the corresponding time series may be parsimoniously described by an LRC model. This applies to just over half the latitudes analyzed. There is clear evidence of LRC at certain latitude bands, while at other latitude bands the autocorrelation behavior is not significantly different from the AR model. Interestingly, the latitudinal structure of LRC behavior is quite different in the two hemispheres.

[23] It should be emphasized that the LRC methods discussed here are based on asymptotic approximations at low frequencies, and therefore they could be sensitive to the frequency interval used for the parameter estimation as follows: a wider interval may yield a bias in the estimates, while a narrower interval results in larger uncertainties of the estimates. Figure 5 is similar to Figure 4, except that GPHE and GSPE were applied to the entire frequency bandwidth from 2 months to 27 years [The results for the AR(1) model (red circles) are identical to those shown in Figure 4]. The Hurst exponents shown in Figure 5b are almost everywhere greater than one; that is, they belong to a nonstationary range. However, Figures 2g, 2h, and 2i demonstrate that the periodograms for the zonal averages have steeper slopes for the bandwidth 2 months to 1 year than for the bandwidth 1–27 years. Therefore the fact that the calculated Hurst exponents are greater than one in this case is an artifact of including the high-frequency (subannual) part of the spectrum in the fit.

[24] To investigate the dependence of the residuals on the definition of the long-term trend, the calculations were repeated but with the residuals defined by using the PWLT in (1) instead of the EESC time series. The results are shown in Figure 6 and may be compared with Figure 4. In the Southern Hemisphere the statistical parameters (and their latitudinal variations) are very similar in the two cases. However, there is a distinct change in the Northern Hemisphere, where the Hurst exponents decrease by about 0.1. Over a broad region of the midlatitudes H is no longer significantly different from 0.5, implying the loss of LRC in this region, and at the highest subpolar latitudes, the extent of LRC behavior is strongly reduced. Inspecting Figure 1f, corresponding to 55°–60°N, it is evident that the major low-frequency variation in the residual defined relative to EESC projects strongly on a piecewise-linear trend with a turning point in early 1996, and its contribution to the residual is therefore substantially reduced when the PWLT function is used to define the long-term trend. This is illustrated by Figure 7, which shows the ozone time series for 55°–60°N (with mean, solar, QBO, and seasonal cycle filtered out) together with the EESC and PWLT fits (Figure 7a) and the PWLT residual (Figure 7b); the latter may be compared with the EESC residual shown in Figure 1f.

4. Significance of Long-Term Trends in Zonal-Mean Total Ozone

4.1. Long-Term Ozone Decline

[25] The statistical model used to describe the noise does not affect the mean trend estimated by equation (1), but it

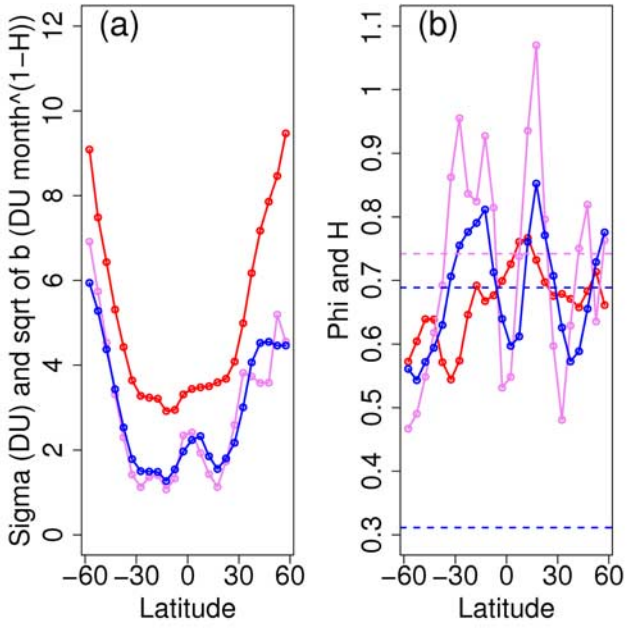

Figure 6. Same as Figure 4, but with PWLT filtered out instead of EESC to describe the long-term trend. The Hurst exponents are similar to those in Figure 4 in the Southern Hemisphere, but are reduced in magnitude by about 0.1 in the Northern Hemisphere.

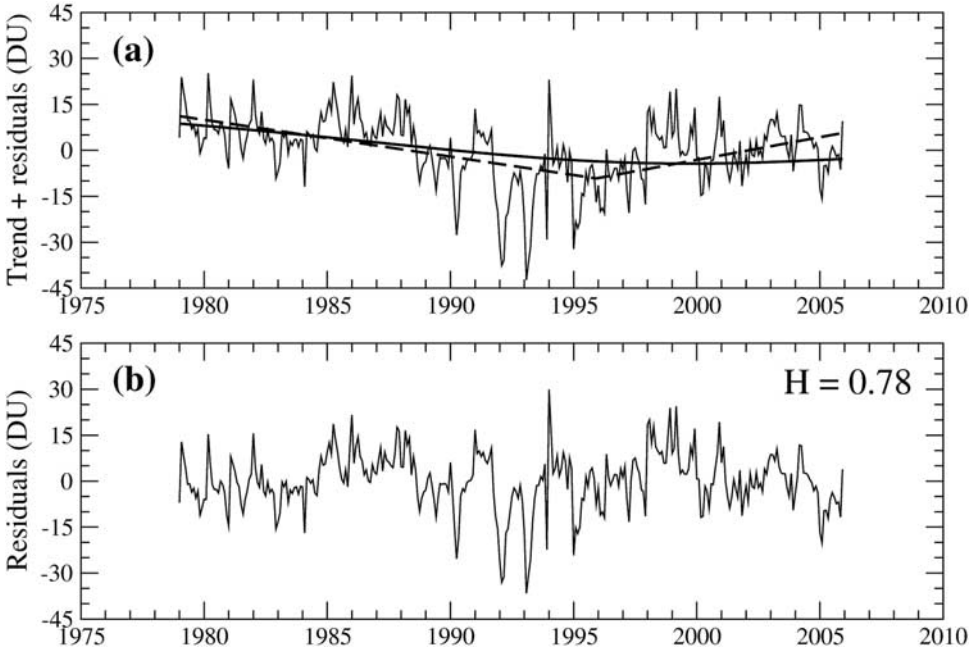

Figure 7. (a) Monthly and zonal mean total ozone anomalies for the 55°–60°N latitude band obtained by filtering out the seasonal cycle, QBO, and solar flux, together with the EESC (solid) and PWLT (dashed) fits. (b) The corresponding total ozone residuals when the PWLT fit is removed. Figure 7b may be compared directly with the EESC-based residuals shown in Figure 1f.

does affect the estimated uncertainty of the trend. The regression coefficient of the total ozone anomalies on the EESC time series is shown in Figure 8a as a function of latitude for the period 1979–2005. The magnitude of the regression coefficient basically displays the sensitivity of total ozone in that latitude band to the stratospheric abundance of ozone-depleting substances as represented by the EESC. For comparison with other estimates the result is presented in Dobson units per year for the time period 1979–1995, during which the EESC time series is nearly linear with a net change of approximately 1.6 ppb of chlorine. As is well known, the long-term ozone decline has a minimum in the tropics and increases toward the poles, with larger values in the Southern Hemisphere as compared with the Northern Hemisphere midlatitudes. The strong increase of the Southern Hemisphere trend with latitude is indicative of the large influence of Antarctic ozone loss on the Southern Hemisphere midlatitude long-term decline [e.g., *Chipperfield*, 2003, *Fioletov and Shepherd*, 2005].

[26] The error bars in Figure 8a indicate the 95% confidence intervals estimated under AR(1) and LRC hypotheses concerning autocorrelation of the residuals. The trend uncertainties under the LRC hypothesis are evidently wider than those under the AR(1) hypothesis. The differences are particularly large where H exceeds 0.7, which, from Figure 4b, occurs basically everywhere north of 35°S. In this region the standard deviation of the trend under the LRC hypothesis is up to 1.5 times larger than that under the AR(1) hypothesis. This broadens the range of tropical latitudes over which the trend is not significant at the 95% level and substantially increases the already large trend uncertainty in northern middle and high latitudes. In contrast, the Hurst exponent is about 0.5–0.6 over the southern middle and high latitudes, i.e., the residuals have relatively weak long-range correlations, and in this region, the trend uncertainties estimated under the LRC and AR(1) hypotheses are nearly identical.

[27] Figure 8b shows the corresponding results for the linear trend from 1979 to 1995 (the declining part of the PWLT function). The means and standard deviations [including the differences between the latter for LRC and AR(1) hypotheses for the residuals] are very similar to those obtained using the EESC fit in Figure 8a, except in northern middle and high latitudes where the PWLT-derived trend is larger. This is consistent with the behavior already noted in section 3.3, where the strong decline in total ozone in northern middle and high latitudes in the early 1990s and its subsequent increase in the late 1990s is interpreted as LRC noise relative to the EESC time series, but contributes to the long-term decline (with weaker LRC behavior in the noise) under PWLT.

4.2. Recent and Future Ozone Increase

[28] The EESC time series can be well approximated by two linear functions, with the first slope equal to about 1 ppb/decade for the period before the EESC maximum in the second half of the 1990s and the second slope equal to about −0.34 ppb/decade for the period after the EESC maximum.

[29] Therefore it is possible to estimate the expected rate of ozone increase after the late 1990s from the EESC fit: It is just the regression coefficient plotted in Figure 8a multiplied by −0.34. The result is shown in Figure 9 by the dotted-dashed curve. For comparison, the positive trend estimated from PWLT, which is the observed linear trend over the time period 1996–2005, is shown by the diamonds connected by the solid curve together with its uncertainties under both the AR(1) and LRC hypotheses. The two trends

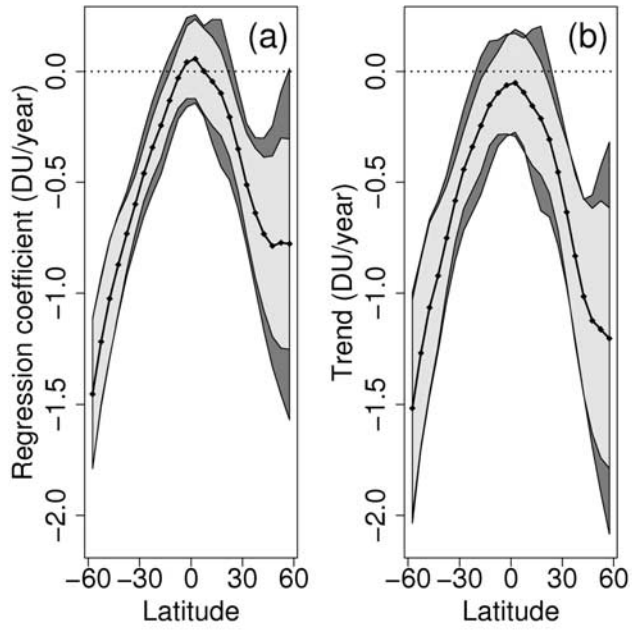

Figure 8. (a) Regression coefficients of monthly and zonal mean total ozone anomalies (obtained by filtering out the seasonal cycle, QBO, and solar flux) on EESC for the period 1979–2005. (b) The first (declining) slope of the PWLT fit for the period 1979–1995. The regression coefficients in Figure 8a are scaled so as to be comparable to the linear trend over 1979–1995; thus the two panels represent, respectively, the EESC-based and PWLT-based estimates of the long-term ozone decline. The 95% confidence intervals shown are calculated under the following two alternative assumptions: AR(1) (light grey region) and LRC (dark grey region). Details of the confidence-interval calculations can be found in Appendix C.

are fairly similar in southern middle and high latitudes, although the uncertainties on the observed trends encompass zero. In northern middle and high latitudes, however, the observed linear trend is roughly four times the EESC-predicted trend and is actually statistically significant over 40°–50°N according to the PWLT estimate of the noise. Thus, once again in northern middle and high latitudes, we have a major difference between the analysis provided by the EESC- and PWLT-based models, although this difference is within the 95% error bars.

[30] Once the analytical relation between the trend uncertainty and the length of the time series is known, it is possible to calculate the number of years required to detect a certain trend with a given error and its dependence on location. This is important from a practical point of view for designing an ozone-monitoring strategy. The number of years required to detect future ozone trends was studied by *Weatherhead et al.* [2000] using the AR(1) model. Here we expand on Weatherhead et al.'s results by including an allowance for LRC behavior. The methods and formulas used here to calculate the number of years are described in Appendix C.

[31] We first consider the number of years required to detect a trend of a given magnitude, without reference to the magnitude of the expected trend. With the noise estimated relative to the EESC trend function (as in Figure 4), the number of years required to detect a 1 DU/year trend in zonal mean total ozone at the 95% significance level under the AR(1) and the LRC hypotheses is shown in Figure 10a. The latitudinal structure primarily reflects that of the variability (cf. Figure 4a), with the shortest number of years being required in the tropics (30°S–30°N). However, the impact of long-term memory (cf. Figure 4b) mainly accounts for the hemispheric asymmetry in Figure 10a, increasing the number of years required in northern as compared with southern latitudes. In those latitude bands for which the Hurst exponents are below 0.7, both the AR(1) and LRC models give consistent estimates of the number of years required, whereas, in other latitude bands, and especially in northern subtropical and high-subpolar latitudes, LRC behavior considerably lengthens the time required to detect a given trend by a factor of up to 1.5 or so.

[32] If the noise is estimated according to the PWLT trend function (as in Figure 6), then the number of years required to detect a 1 DU/year trend is virtually identical to that shown in Figure 10a in the Southern Hemisphere, but is, as expected, reduced and closer to that estimated from the AR(1) model in the Northern Hemisphere (not shown). Figure 10b shows the same estimates as in Figure 10a, except that, in estimating the statistical parameters b and H under the LRC hypothesis, GPHE and GSPE were applied to the frequency bandwidth from 2 months to 27 years (cf. Figure 5). The number of years in this case is several times larger than for the proper bandwidth (1–27 years). We include Figure 10b here to emphasize the importance

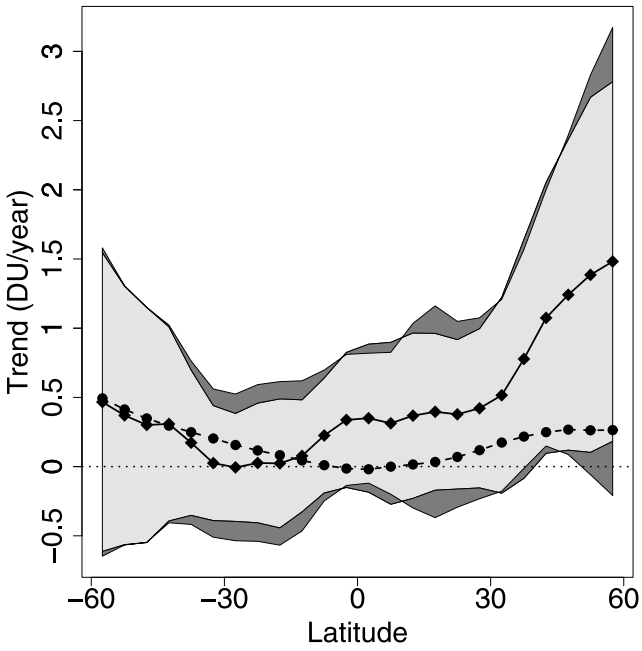

Figure 9. The EESC-based linear trend calculated for the declining part of EESC (solid circles connected by the dashed line) is compared to the second (increasing) slope of the PWLT fit for the period 1996–2005 (diamonds connected by the solid line), the latter with 95% confidence intervals calculated under the AR(1) (light grey region) and LRC assumptions (dark grey region).

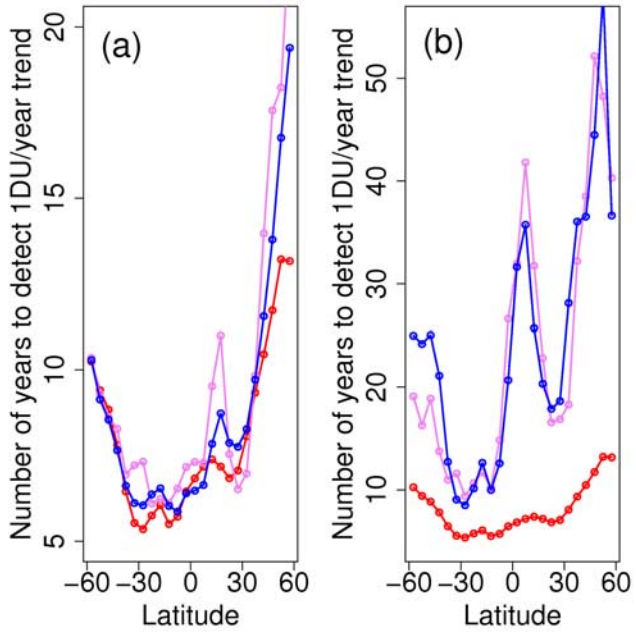

Figure 10. (a) The number of years required to detect a 1 DU/year trend at the 95% significance level under the AR(1) (red curve) and LRC assumptions (violet curve shows GPHE, blue curve shows GSPE) applied to the frequency bandwidth 1–27 years of the monthly mean total ozone residuals obtained by filtering out the seasonal cycle, QBO, solar flux, and EESC fit. (b) The same as Figure 10a, but using the frequency bandwidth 2 months to 27 years for the LRC estimates (the red curve is the same in both panels). Note the different vertical scales in the two panels. Figure 10b is a spurious result (cf. Figure 5) and is shown to highlight the importance of choosing an appropriate bandwidth for the analysis.

of a correct bandwidth choice for Hurst exponent estimation under the LRC model.

[33] We now consider the latitudinal dependence of the expected trends, and estimate the number of years required to detect a statistically significant ozone increase if the positive trends are those estimated in Figure 9 according to either the EESC or PWLT models. In both cases the "detection" is made here under the assumption that the trend is independent of the past trend (prior to 2000 for EESC, prior to 1996 for PWLT), and both AR(1) and LRC estimates are computed. Consider first the detection of the positive ozone trend expected from the EESC decline, shown in Figure 11a. As was noted by *Weatherhead et al.* [2000], southern middle and high latitudes are the best places to detect ozone recovery according to the AR(1) model; the same is seen to be true for the LRC model. In the Northern Hemisphere, there appears to be an optimal region for detection of ozone recovery around 30°–40°N; on either side, there is a strong effect of LRC behavior on the number of years required, especially at northern middle and high latitudes where, according to the LRC model, it should take about 1.5 times longer to detect the expected trends than estimated under the AR(1) model.

[34] The number of years required to detect the observed trend from 1996 to 2005 at the 95% significance level, according to the PWLT analysis, is shown in Figure 11b. The length of the observed record (10 years) is indicated by the dotted line; at latitudes with points lying below this line, a significant trend has therefore already been detected (cf. Figure 9). The result is completely different from Figure 11a. According to the PWLT analysis, the best place to detect ozone recovery is northern middle and high latitudes (moreover, in this region, a positive trend is either on the verge of being detected or has already been detected) and the second best region is in the equatorial zone. However, at southern high latitudes, the number of years required, ~18, is similar between the EESC and PWLT analyses and is well estimated by the AR(1) model in both cases. This is expected given the consistency at these latitudes of the EESC-predicted and observed recent trends, the consistency of the EESC- and PWLT-derived noise estimates, and the absence of LRC.

5. Longitudinal Structure

[35] In this section we present the latitude-longitude distributions of some of the statistical parameters discussed above for zonal averages. Figures 12a and 12b show the spatial distributions of the AR(1) month-to-month autocorrelation parameter ϕ and the Hurst exponent H, respectively,

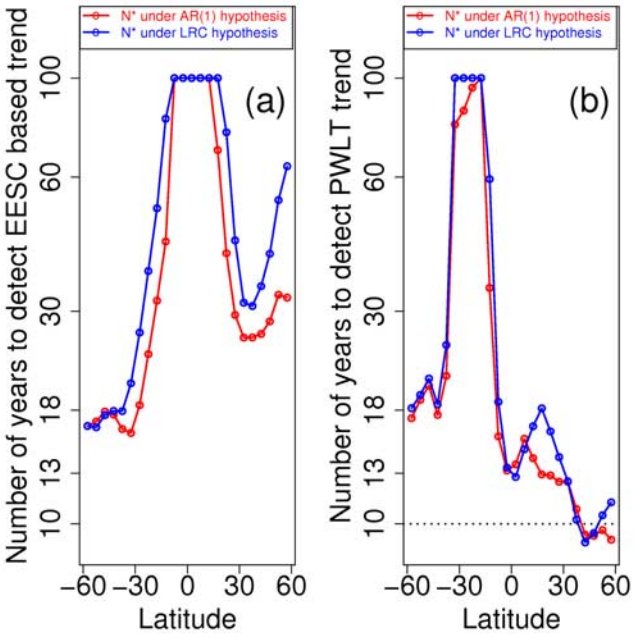

Figure 11. (a) The number of years since 2000 required to detect the EESC-based linear trend calculated for the declining part of EESC at the 95% significance level under the following two alternative assumptions: AR(1) (red curve) and LRC (blue curve, based on GSPE). (b) The same as Figure 11a, but for the PWLT-based trend calculated for the period 1996–2005, so the value represents the number of years after 1996. Values higher than 100 years are plotted as 100 years. Note the similarity of the two estimates in southern middle and high latitudes, but the large differences in the Northern Hemisphere. See text for details.

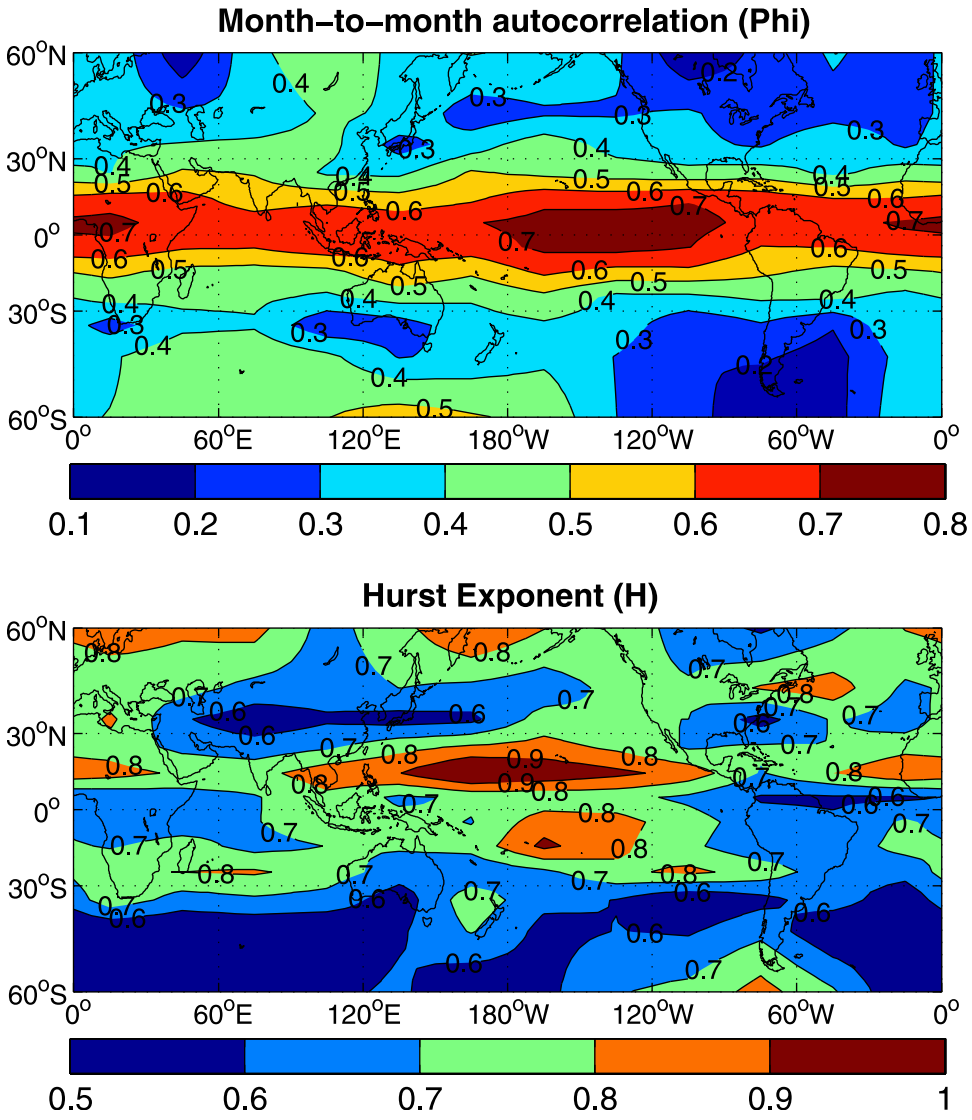

Figure 12. Spatial distribution of the month-to-month autocorrelation parameter ϕ (top panel) and the Hurst exponent (bottom panel) calculated by GSPE for monthly mean total ozone residuals obtained by filtering out the seasonal cycle, QBO, solar flux, and EESC fit. This is the two-dimensional version of Figure 4b.

when the trend is defined by the EESC function. Both ϕ and H reflect "memory" in the total ozone time series but there is a distinct difference in their spatial structure. The autocorrelation parameter has its maximum at the equator and decreases toward the poles; the values are very similar to those reported by *Weatherhead et al.* [2000, Figure 4, Plate 3] for 1979–1998. In contrast, the spatial distribution of the Hurst exponent has two maxima, around 15°S over the Pacific and 20°N over the Pacific, eastern Atlantic, and Africa. For both ϕ and H, the maxima have pronounced longitudinal structure. The values of H for zonal-mean ozone (Figure 4b) are approximately equal to the maximum values of H for gridded ozone at the given latitude, consistent with the arguments of *Granger* [1980]. The spatial distribution of the Hurst exponent when the PWLT is filtered out instead of EESC (not shown) is similar to Figure 12b, except that the values are lower in the Northern Hemisphere.

[36] Figures 13a and 13b show the spatial distributions of the recent trends according to the EESC and PWLT functions, respectively; they correspond to the curves in Figure 9 for zonal-mean ozone. In the case of EESC, this represents the positive linear trend expected since the late 1990s based on the fitting of the entire 1979–2005 record by the EESC time series. On the basis of EESC, the ozone recovery rate should be strongest in the Southern Hemisphere subpolar regions, apart from the south-west Pacific. In the Northern Hemisphere the recovery rate is predicted to be relatively strong over northern Europe and over eastern Siberia. In the tropics and subtropics the expected recovery rate is weak and very zonal. As can be anticipated from Figure 9, the ozone recovery rates based on PWLT (i.e., the observed linear trend from 1996–2005) are also positive everywhere but have a very different spatial distribution and strength. In particular, the PWLT recovery rates are greater in the Northern Hemisphere midlatitudes and subpolar regions than

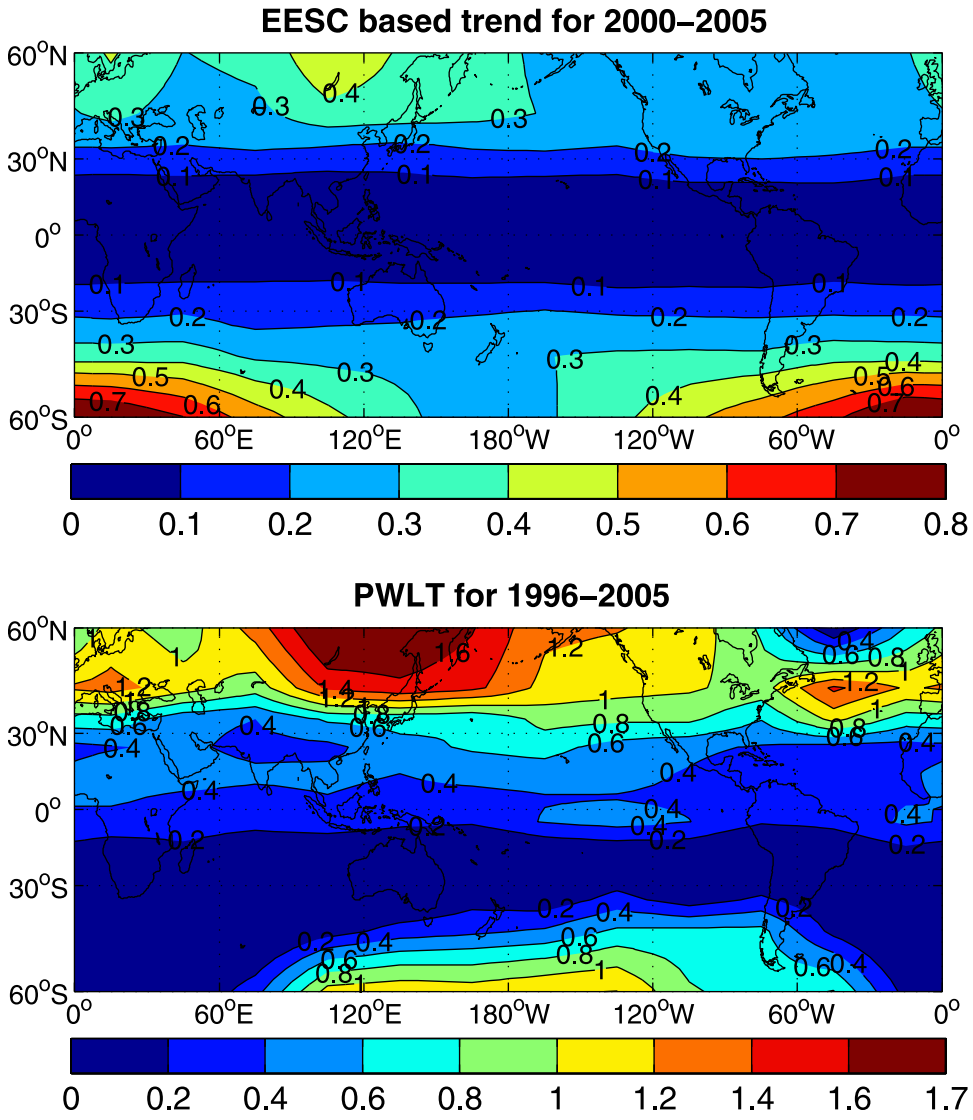

Figure 13. Spatial distribution of the EESC-based linear trend calculated for the declining part of EESC in DU/year (top panel) and the second (increasing) slope of the PWLT fit for the period 1996–2005 (bottom panel). This is the two-dimensional version of Figure 9.

in the Southern Hemisphere; the trends are especially strong over Siberia, the North Pacific, the northern midlatitude Atlantic, and Europe. The only place in the Northern Hemisphere midlatitudes and subpolar regions where the trends are relatively weak is the subpolar North Atlantic. The spatial distribution of the recent PWLT over the southern ocean is opposite to that for the EESC trend, with a maximum rather than a minimum over the south-west Pacific.

[37] Finally, Figure 14 presents the number of years from the year 2000 required to detect the expected EESC-based ozone trends shown in Figure 13a, based on the LRC noise estimates computed from the entire time series (with the EESC trend filtered out). The Figure allows us to identify the optimal locations to make long-term ground-based total ozone observations. For example, it would be desirable to have some stations in the southern subpolar Atlantic since the number of years required to detect ozone recovery has a minimum in that region, where it varies between 12 and 20 years. In the Northern Hemisphere the minimum is located in the zonal band around 35°N and varies between 20 and 30 years.

6. Summary and Discussion

[38] The statistical analysis of long-term changes in total ozone has traditionally been performed assuming that the residuals, which represent the noise in the system, are well described by an AR(1) model. In this study the total ozone record from 1979 to 2005 has been examined for the existence of long-range correlations (LRC), implying a deviation from AR(1) behavior with an unbounded decorrelation time. The existence of LRC behavior in total ozone would reduce the statistical significance of a given trend, and lengthen the number of years required to detect a trend, from that estimated using an AR(1) model. We employ the merged satellite data set prepared by NASA which combines version 8 of TOMS and SBUV total ozone data [*Frith et al.*, 2004; *Stolarski and Frith*, 2006], use well-based spectral estimation techniques to quantify LRC paying

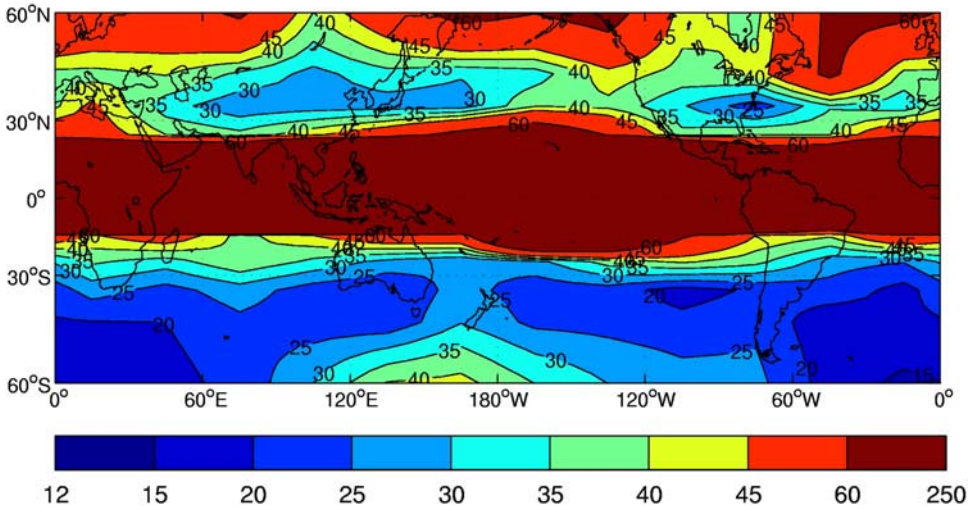

Figure 14. The number of years since 2000 required to detect the EESC-based linear trend calculated for the declining part of EESC at the 95% significance level under the LRC assumption (based on GSPE). This is the two-dimensional version of Figure 11a.

proper attention to the frequency bandwidth, and filter long-term time periodic signals (QBO, solar) which can give spurious indications of LRC behavior. The analysis mainly concerns zonal-mean ozone, although some station data and gridded satellite data are also considered. However, the analysis is restricted to 60°S–60°N, as, in polar regions, the satellite data have gaps during polar night.

[39] We first summarize the results obtained when the long-term total ozone changes are represented in terms of the EESC time series. Clear evidence of LRC is found basically everywhere north of 35°S. In the southern middle and high latitudes the correlation behavior is not significantly different (at the 95% significance level) from that of the AR(1) model. In the regions with strong LRC behavior, uncertainties in the magnitude of the long-term ozone decline attributable to EESC are increased by about a factor of 1.5 compared with those estimated from AR(1); this includes the northern middle and high latitudes, where the AR(1)-based uncertainties are already quite large. However, the strongest long-term ozone decline is found at the southern middle and high latitudes, and there, the AR(1) estimates are found to be reliable.

[40] Analogous results are found for the number of years (from 2000) required to detect the increase of ozone expected from the anticipated decline of EESC. We confirm *Weatherhead et al.*'s [2000] finding, on the basis of the AR(1) model, that southern middle and high latitudes should be the optimal place (within the 60°S–60°N region) to detect ozone increase; at these latitudes, we have the combination of the strongest expected trend, the apparent absence of LRC behavior, and the shortest autocorrelation times. The required detection time (to 95% significance) is about 18 years for zonal-mean ozone at 60°S, but is even a few years shorter in the subpolar South Atlantic. While limited regions have higher noise levels, they also have weaker serial correlations. The recent observed behavior of total ozone in these regions is consistent with the EESC-predicted trend, but detection of an ozone increase attributable to EESC is not expected until sometime late in the decade 2010–2020. In the Northern Hemisphere, detection of ozone increase is more challenging. There appears to be a narrow band around 35°N where LRC behavior is relatively weak and the required number of years is around 30, but in northern middle and high latitudes, the required number of years is increased from around 25–35 to around 30–60 by LRC.

[41] Although the representation of long-term ozone changes in terms of the EESC time series is preferred, given the a priori nature of the representation, a commonly used alternative is a piecewise-linear trend (PWLT) with a turning point in the second half of the 1990s. Therefore we compared the results obtained using the two different representations of the long-term changes. In our implementation of PWLT we use a turning point in early 1996. The estimates of the noise and the long-term ozone decline are essentially the same for the two cases in the Southern Hemisphere, but there is a notable discrepancy in the Northern Hemisphere (particularly at northern middle and high latitudes) where the strong decrease in ozone in the early 1990s, and its subsequent increase in the late 1990s, are interpreted mainly as LRC noise relative to EESC, but project strongly on the long-term changes (thereby reducing the strength of the LRC behavior) relative to the PWLT. This difference affects all subsequent estimates. For example, according to PWLT, the long-term ozone decline in northern middle and high (subpolar) latitudes is comparable in magnitude to that in the Southern Hemisphere; the recent ozone increase (since 1996) is strongest in this region, and marginally statistically significant (at the 95% significance level) indicating that a positive ozone trend is already on the verge of being detected.

[42] The natural question is, then, which representation of the long-term changes (and thus of the noise) is correct? We do not attempt to answer this question definitively, but a few comments may be in order. If one adopts the EESC perspective, then the results seem physically sensible as follows: we know that the annual-mean long-term ozone decline, from pre-1980 levels to those characteristic of the 2000 time period, over the middle and high (subpolar)

latitudes has been much greater in the Southern Hemisphere as compared with the Northern Hemisphere, roughly 6% as compared with 3% [*WMO*, 2003]. Furthermore, we know that the Northern Hemisphere ozone exhibits more interannual variability than the Southern Hemisphere ozone because of the greater stratospheric dynamical variability in the Northern Hemisphere, which is for well-understood reasons. What remains then to be understood is the physical origin of the LRC, especially in northern middle and high latitudes. If it is the existence of AR timescales comparable to the 27-year observational record, then are these timescales associated with natural variability or with climate change? These questions can likely only be answered with climate models.

[43] If, on the other hand, one adopts the PWLT perspective, then one is forced to consider the strong decline of northern middle and high latitude ozone in the early 1990s, and its subsequent increase in the late 1990s, as part of the signal and account for it. One possibility often considered [e.g., *Solomon et al.*, 1996] is that the increased stratospheric aerosol from the Mount Pinatubo volcanic eruption in 1991 amplified the EESC-associated ozone loss. The problem with this argument is that there was no corresponding ozone decrease observed in the Southern Hemisphere, even though EESC and aerosol abundances were comparable [*Bodeker et al.*, 2001]. Another argument is that the behavior reflects decadal-scale variations in stratospheric wave forcing [e.g., *Randel et al.*, 2002; *Hadjinicolaou et al.*, 2005], which would affect ozone both through changes in transport and changes in chemical ozone loss, especially in the Arctic which would then affect the annual mean subpolar ozone abundances through the transport of ozone-depleted air. The impact of long-term changes in stratospheric wave forcing on both polar and midlatitude ozone is well established [*WMO*, 2003]. However, attributing the ozone changes to changes in wave forcing merely changes the problem to that of accounting for the variations in wave forcing. In principle, they could be part of the signal or part of the noise. Yet the use of PWLT involves the implicit assumption that the recent strong positive trend in northern middle- and high-latitude ozone is secular and can be extrapolated; moreover, by regarding this trend as part of the signal rather than part of the noise, the estimated noise is reduced and the LRC behavior weakened, and the estimated significance of the trend thereby increased. So far, no mechanism that could give such a statistically significant positive trend in the northern middle and high latitude ozone has been put forward.

Appendix A: Introduction to Long-Range Correlated Processes

[44] Development of the theory for a class of stochastic processes with long-range correlated increments was originated by Kolmogorov in two short notes [*Kolmogorov*, 1940a, 1940b] during his studies of turbulence. The seminal paper of *Mandelbrot and Van Ness* [1968] developed many of its properties and named it by the class of self-similar processes.

[45] A real-valued stochastic process $Z=\{Z(t)\}_{t\in\mathbb{R}}$ is self-similar with index $H > 0$ if, for any $a > 0$,

$$\{Z(at)\}_{t\in\mathbb{R}} \stackrel{d}{=} \{a^H Z(t)\}_{t\in\mathbb{R}}, \tag{A1}$$

where $\stackrel{d}{=}$ denotes the equality of the finite-dimensional distributions [*Taqqu*, 2002]. In this article we use increments of a self-similar process for modeling residuals of the total ozone time series. The autocovariance of the increment sequence $X_i = Z_i - Z_{i-1}$ of a self-similar process

$$\gamma(t) = cov(X_i, X_{i+t}) = \frac{\sigma^2}{2}\left[|t+1|^{2H} - 2|t|^{2H} + |t-1|^{2H}\right]$$

asymptotically decays by a power law [e.g., *Beran*, 1994]

$$\gamma(t) \sim \sigma^2 H(2H-1)|t|^{2H-2}, \text{ as } t \to \infty. \tag{A2}$$

[46] The increments of a self-similar stochastic process for $1/2 < H < 1$ have long-range correlated behavior, since $\gamma(t)$ decays to zero so slowly that $\sum_{t=-\infty}^{\infty}\gamma(t)$ diverges. There are no long-range correlations in the "blue" noise case ($H < 0.5$). Usually for climatic time series $0.5 \le H < 1.0$. The case $H = 0.5$ corresponds to short-memory processes, which can be well modeled by conventional autoregressive moving average (ARMA) models. Spectral density of the increment sequence of a self-similar process scales by a power law in the vicinity of the origin

$$f_X(\lambda) = b|\lambda|^{1-2H}, \text{ as } \lambda \to 0. \tag{A3}$$

[47] The next appendix provides an overview of spectral statistical methods for estimating parameters b and H of a given time series.

Appendix B: Statistical Methods for Estimation of *b* and *H*

[48] In the beginning of the estimation process, one calculates the discrete Fourier transform of a given time series

$$w(j) = \frac{1}{\sqrt{2\pi n}}\sum_{t=1}^{n} X(t)e^{it\frac{2\pi j}{n}}, \quad j = 1..[n/2], \tag{B1}$$

where square brackets denote rounding toward zero, and the periodogram—an estimate of the spectral density

$$I(j) = |w(j)|^2 = \frac{1}{2\pi n}\left|\sum_{t=1}^{n} X(t)e^{it\frac{2\pi j}{n}}\right|^2, \tag{B2}$$

where n is the time series length. The goal is to approximate the estimate of the spectral density $I(j)$ by an analytical form for the spectral density, in our case $f(b, H, \lambda) = b|\lambda|^{1-2H}$, where $\lambda = 2\pi j/n$. There are several semiparametric methods for estimating b and H. For a recent review, see for instance *Moulines and Soulier* [2002]. Many of them might be described in terms of the so-called contrast function $k(u, v)$, which can be thought of as a distance between functions u and v. Then the approximation process reduces to minimization of the following functional

$$K(b,H) = \frac{1}{m}\sum_{j=1}^{m} k\left(I(j), f\left(b, H, \frac{2\pi j}{n}\right)\right), \tag{B3}$$

where $1 < m \le [n/2]$ is an index of the highest frequency used. The meaning of the free parameter m is similar to the

order of autoregressive fractionally integrated moving average (ARFIMA) model. However, in contrast to the order of ARFIMA, m has a clear physical sense. For instance, in our study, we focus mainly on interannual variability of the monthly resolved total ozone and thus choose $m = n/12$. In sections 3.3 and 4.2, we compared some results for $m = n/2$ (full spectrum) and $m = n/12$. In this article we apply the following two methods of semiparametric estimation: Geweke-Porter-Hudak estimator (GPHE) and Gaussian semiparametric estimator (GSPE). GPHE was originally proposed by *Geweke and Porter-Hudak* [1983] and probably is the most popular, because of its simple realization, semiparametric estimator used in applications. GPHE corresponds to the contrast function $k(u, v) = (\log(u) - \log(v))^2$. Therefore it simply performs a log linear regression of the periodogram. For GPHE parameters b and H, which minimize $K(b, H)$, can be found in a closed form. The graphical illustration of GPHE is shown in Figure 2. A more advanced estimator, GSPE, was introduced by *Fox and Taqqu* [1988]. Its contrast function is $k(u, v) = \log(u) + u/v$. GSPE is a maximum likelihood estimator. For GSPE the problem of minimization of $K(b, H)$ can be reduced to a one-dimensional minimization problem and solved using standard optimization technique. Rigorous mathematical justification of GPHE and GSPE was given by *Robinson* [1995a, 1995b], respectively. Robinson showed that GSPE is superior to GPHE. For instance, it has by a factor of $\pi^2/6$ smaller asymptotic variance. In practice, we find that GSPE gives less noisy (spatially) and more robust estimates than GPHE.

Appendix C: Trend Variance and the Number of Years Required to Detect a Trend

[49] For the purpose of trend analysis, memory is an issue. It is hard to distinguish a trend from natural variability in case time series is strongly serially correlated. The importance of taking into account LRC in trend analysis was first realized by *Bloomfield* [1992] during his studies of trends in surface air temperature. He proposed to use autoregressive fractionally integrated moving average (ARFIMA) model, introduced independently by *Granger and Joyeux* [1980] and *Hosking* [1981], for modeling temperature residuals. The idea is to fit the residuals, obtained after filtering out deterministic components of temperature time series such as seasonal cycle and trend, by ARFIMA and, knowing analytical expression for the variance of ARFIMA, calculate the variance of the trend. Bloomfield's approach can be classified as sequential full parametric estimation, since one first estimates and filters out the trend and then estimates the parameters of ARFIMA. Joint full parametric estimation, when the trend and the parameters of ARFIMA are estimated simultaneously, was theoretically justified by *Robinson* [2005] and was applied to Northern Hemisphere SAT anomalies by *Gil-Alana* [2005]. The disadvantage of full parametric approach for trend detection studies is a problem of choosing the correct order of the ARFIMA, which itself is an issue [*Beran et al.*, 1998]. An appealing way to overcome the issue of model selection was proposed by *Smith* [1993]. He showed that it is important to fit only the low-frequency part of the residuals' spectrum using an asymptotic form of LRC spectral density $f(\lambda) = b|\lambda|^{1-2H}$ with only two unknown parameters. Then the variance of the trend can be calculated on the basis of these two parameters. We follow this direction in our paper. This approach is classified as semiparametric since it requires estimation only of a part of the whole parameter set. *Smith and Chen* [1996] advocated for joint estimation of the trend and the parameters b and H. Unfortunately, this theoretically more correct approach is still missing a solid mathematical foundation. Therefore, in our article, we implement sequential semiparametric estimation; that is, we first estimate and filter out the trend from the time series and then find b and H for the residuals using semiparametric estimation. The general theoretical justification of this method is given by *Yajima* [1988].

C1. Estimation of Trend Variance Through Autocovariance

[50] Let's consider a general linear estimator

$$\hat{\xi} = \sum_{t=1}^{n} l(t) Y(t). \tag{C1}$$

Variance of $\hat{\xi}$ may be expressed through autocovariance γ of $Y(t)$

$$\sigma^2\left(\hat{\xi}\right) = \sum_{t=1}^{n} \sum_{s=1}^{n} l(t) l(s) \gamma(t-s). \tag{C2}$$

For example, for the statistical model

$$Y(t) = \alpha + \beta y(t) + X(t), \tag{C3}$$

where $y(t)$ is a certain explanatory variable (covariate) with zero mean and $X(t)$ is a noise, the slope estimator $\hat{\beta}$ and its variance $\sigma^2(\hat{\beta})$ may be written as follows

$$\hat{\beta} = \frac{\sum_{t=1}^{n} y(t) Y(t)}{\sum_{t=1}^{n} y^2(t)}, \tag{C4}$$

$$\sigma^2\left(\hat{\beta}\right) = \frac{\gamma(0) \sum_{t=1}^{n} y^2(t) + 2 \sum_{k=1}^{n-1} \gamma(k) \sum_{j=1}^{n-k} y(j) y(j+k)}{\left(\sum_{t=1}^{n} y^2(t)\right)^2}, \tag{C5}$$

where n is the time series length; $\gamma(t)$ is the residuals' autocovariance function.

C2. Approximation of Autocovariance by Exponential Function

[51] The most conventional way to proceed from this point is to use an exponential approximation for the residuals' autocovariance function $\gamma(t)$ for deriving an asymptotic formula for $\sigma(\hat{\beta})$. In principle, one can use the estimate of $\gamma(t)$ to numerically evaluate $\sigma(\hat{\beta})$. However, because of poor sampling properties of autocovariance function estimates, statisticians prefer to use a certain approximation

of sample autocovariance function. To obtain an exponential approximation for the autocovariance function, one can fit an autoregressive model of the first order [AR(1)] to the noise. Symbolically, AR(1) can be written as follows:

$$X(t) = \phi X(t-1) + \varepsilon(t), \tag{C6}$$

where $-1 < \phi < 1$ is month-to-month autocorrelation (lag-one autocorrelation coefficient) and $\varepsilon(t)$ is a Gaussian white noise. Let's review some of the AR(1) model properties. Autocovariance function of AR(1) decays exponentially

$$\gamma_{\mathrm{AR1}}(t) = \sigma_X^2 \phi^{|t|}. \tag{C7}$$

Spectral density of AR(1)

$$f_{\mathrm{AR1}}(\lambda) = \frac{\sigma_X^2}{2\pi} \frac{1-\phi^2}{|1-\phi e^{-i\lambda}|^2} \rightarrow \frac{\sigma_X^2}{2\pi} \frac{1+\phi}{1-\phi}, \text{ as } \lambda \rightarrow 0,$$

where σ_X is the standard deviation of $X(t)$.

[52] In case we assume an AR(1) model for the monthly resolved residuals $X(t)$ and take $y(t) = t - (n+1)/2$, we have

$$\sigma_{\mathrm{AR1}}(\hat{\omega}) \approx \frac{\sigma_X}{N^{3/2}} \sqrt{\frac{1+\phi}{1-\phi}}, \tag{C8}$$

where $\hat{\omega} = 12\hat{\beta}$ is the estimate of the linear trend in unit $y(t)$ per year; N is the length of a considered period in years [*Weatherhead et al.*, 1998].

C3. Approximation of Autocovariance by Power Law Function

[53] The alternative approach is to use a power law approximation of the sample autocovariance function whose coefficients can be obtained by various estimation methods (see Appendix B). Substituting $\gamma(0) = \sigma_X^2$, $\gamma(t) = at^{2H-2}$ for $t > 0$, and $y(t) = t - (n+1)/2$ into equation (C5) and performing asymptotic derivations we obtain

$$\sigma^2\left(\hat{\beta}\right) \approx \frac{36a(1-H)}{H(1+H)(2H-1)} n^{2H-4}. \tag{C9}$$

Scaling factors of the autocovariance and the spectral density, a and b, are related as follows [e.g., *Smith*, 1993]:

$$a = \frac{\pi b}{\Gamma(2H-1)\sin(\pi H)}. \tag{C10}$$

Using this relation and some properties of the gamma function we can rewrite the asymptotic formula for $\sigma(\hat{\beta})$ in terms of b and H

$$\sigma_{\mathrm{LRC}}\left(\hat{\beta}\right) \approx B(b,H) n^{H-2}, \tag{C11}$$

where $\sigma_{\mathrm{LRC}}(\hat{\beta})$ is the standard deviation of the estimated trend under the LRC hypothesis and

$$B(b,H) = \sqrt{\frac{72b\pi(1-H)}{(1+H)\Gamma(2H+1)\sin(\pi H)}}. \tag{C12}$$

Equations (C8) and (C11) were used in Figures 8b and 9.

C4. Estimation of Trend Variance Through Spectral Density

[54] Asymptotic formulas can be derived only in cases when the explanatory variable $y(t)$ has a relatively simple form such as a linear trend. In other cases, one can estimate the standard deviation of a slope only numerically. From the numerical point of view, it is more convenient to express the autocovariance through the spectral density. Thus replacing in formula (C2) the autocovariance by its expression through the spectral density of $X(t)$

$$\gamma(k) = \int_{-\pi}^{\pi} e^{i\lambda k} f(\lambda) \mathrm{d}\lambda, \tag{C13}$$

we obtain

$$\sigma^2\left(\hat{\xi}\right) = \int_{-\pi}^{\pi} U(\lambda) f(\lambda) d\lambda, \tag{C14}$$

where

$$U(\lambda) = \left| \sum_{t=1}^{n} l(t) e^{i\lambda t} \right|^2. \tag{C15}$$

The important thing is that almost all weight of the function $U(\lambda)$ is concentrated near the origin. Therefore, for the calculation of the trend uncertainty, the high-frequency part of the spectrum is not important. This fact motivates the implementation of semiparametric (local) instead of full parametric (global) statistical models [*Smith*, 1993]. For example, in order to calculate the slope uncertainty in case $y(t) = \mathrm{EESC}(t) - \overline{\mathrm{EESC}(t)}$, where $\mathrm{EESC}(t)$ is the equivalent effective stratospheric chlorine time series, and $f(\lambda) = b|\lambda|^{1-2H}$, we used the following formula:

$$\sigma^2\left(\hat{\beta}_{\mathrm{EESC}}\right) = b \int_{-\pi/12}^{\pi/12} U_{\mathrm{EESC}}(\lambda) |\lambda|^{1-2H} d\lambda, \tag{C16}$$

where

$$U_{\mathrm{EESC}}(\lambda) = \left| \sum_{t=1}^{n} \frac{\mathrm{EESC}(t) - \overline{\mathrm{EESC}(t)}}{\sum_{s=1}^{n} \left(\mathrm{EESC}(s) - \overline{\mathrm{EESC}(s)}\right)^2} e^{i\lambda t} \right|^2.$$

Therefore we could neglect intra-annual variability [frequency ranges $(-\pi/2, -\pi/12)$ and $(\pi/12, \pi/2)$] of the total ozone anomalies. Equation (C16) was used in Figure 8a.

C5. Estimation of the Number of Years Required to Detect a Trend

[55] The number of years required to detect a trend of specified magnitude $|\omega|$ under the hypothesis that $X(t)$ can be well described by an AR(1) model according to *Weatherhead et al.* [1998] is as follows

$$N^*_{\mathrm{AR1}} \approx \left[\frac{(2+z_p)\sigma_X}{|\omega|}\sqrt{\frac{1+\phi}{1-\phi}}\right]^{2/3}, \qquad \text{(C17)}$$

where N^*_{AR1} is the number of years required to detect a trend of specified magnitude $|\omega|$ (in particular, one may choose $\omega = \hat{\omega}$) and z_p is the p percentile of the standard normal distribution.

[56] In this setup the probability to reject the test hypothesis of zero trend when it is true is equal to 5% and the probability to accept the hypothesis of zero trend when it is false is equal to p. The number of years required to detect a linear trend of specified magnitude $|\omega|$ depends on three key parameters in the AR(1) case (ω, σ, ϕ).

[57] From (C11) we derive an analogous equation for the case when $X(t)$ are long-range correlated

$$n^*_{\mathrm{LRC}} \approx \left[\frac{(2+z_p)B(b,H)}{|\beta|}\right]^{\frac{1}{2-H}}. \qquad \text{(C18)}$$

In the above equation, n is expressed in basic time units of time series, i.e., days or months, and β has a unit $y(t)$ per year. Let's now transform this equation to the form which is conventionally used in ozone trend analysis when the time to detect the trend has units of years and the trend has units of Dobson units per year. Let $n = TN$ and $\beta = \omega/T$, where T is the length of year in basic time units, i.e., $T = 365$ or $T = 12$, N is the length of the time series in years, and ω is the trend in Dobson units per year. Then from equation (C18) we get

$$N^*_{\mathrm{LRC}} \approx \left[\frac{(2+z_p)B(b,H)}{|\omega|T^{1-H}}\right]^{\frac{1}{2-H}}. \qquad \text{(C19)}$$

[58] This formula is somewhat similar to formula (C17). However, because of the fact that the exponent in formula (C19) is greater than the corresponding exponent in formula (C17), trend error bars tend to be larger under LRC hypothesis than under AR(1) hypothesis. It means we have to observe the time series longer in order to detect the trend with the same statistical significance. The number of years required to detect a linear trend of specified magnitude $|\omega|$, in case $X(t)$ are LRC, also depends on the following three key parameters: magnitude of the trend $|\omega|$, spectral scaling factor b, and the Hurst exponent. It is worth to note that formula (C19) is a generalization of formula (C17). Thus, for monthly resolved time series ($T = 12$) under assumption of AR(1) model, we get that $H_{\mathrm{LRC}} \rightarrow H_{\mathrm{AR1}} = \frac{1}{2}$,

$$b_{\mathrm{LRC}} \rightarrow b_{\mathrm{AR1}} = \frac{\sigma_X^2}{2\pi}\frac{1+\phi}{1-\phi}, \qquad \text{(C20)}$$

and $B_{\mathrm{LRC}} \rightarrow B_{\mathrm{AR1}} = \sqrt{24\pi b_{\mathrm{AR1}}}$. Therefore formula (C19) reduces to formula (C17). The numerical validation of this fact can be noticed by looking at the Southern Hemisphere middle and high latitudes in Figures 4b, 6b, 8, 9, and 11. The Hurst exponent converges to 0.5 as one moves from 30° to 60°S as shown in Figures 4b and 6b. Simultaneously, the LRC trend error bars converge to the AR(1) errors bars in Figures 8 and 9, and the number of years to detect the trend under LRC hypothesis converges to the one under AR(1) hypothesis in Figures 10a and 11.

[59] **Acknowledgments.** This research has been supported by the Canadian Foundation for Climate and Atmospheric Sciences and the Natural Sciences and Engineering Research Council. We thank the "R Foundation for Statistical Computing" for the R environment and David Pierce for the ncdf package. Dmitry Vyushin is grateful to Paul Kushner and Michael Sigmond for fruitful discussions. Dmitry Vyushin is supported by the Natural Sciences and Engineering Research Council and the Meteorological Service of Canada.

References

Beran, J. (1994), Statistics for Long-Memory Processes, CRC Press, Boca Raton, Fla.

Beran, J., R. I. Bhansali, and D. Ocker (1998), On unified model selection for stationary and nonstationary short- and long-memory autoregressive processes, *Biometrika*, *85*, 921–934.

Bloomfield, P. (1992), Trends in global temperature, *Clim. Change*, *21*, 1–16.

Bodeker, G. E., B. J. Connor, J. B. Liley, and W. A. Matthews (2001), The global mass of ozone: 1978–1998, *Geophys. Res. Lett.*, *28*, 2819–2822.

Chipperfield, M. P. (2003), A three-dimensional model study of long-term mid-high latitude lower stratosphere ozone changes, *Atmos. Chem. Phys.*, *3*, 1253–1265.

Dhomse, S., M. Weber, I. Wohltmann, M. Rex, and J. P. Burrows (2006), On the possible causes of recent increases in Northern Hemispheric total ozone from a statistical analysis of satellite data from 1979 to 2003, *Atmos. Chem. Phys.*, *6*, 1165–1180.

Fioletov, V. E., and T. G. Shepherd (2005), Summertime total ozone variations over middle and polar latitudes, *Geophys. Res. Lett.*, *32*, L04807, doi:10.1029/2004GL022080.

Fioletov, V. E., G. E. Bodeker, A. J. Miller, R. D. McPeters, and R. Stolarski (2002), Global and zonal total ozone variations estimated from ground-based and satellite measurements: 1964–2000, *J. Geophys. Res.*, *107*(D22), 4647, doi:10.1029/2001JD001350.

Fox, R., and M. Taqqu (1988), Large sample properties of parameter estimates for strongly dependent stationary Gaussian time series, *Ann. Stat.*, *17*, 1749–1766.

Frith, S., R. Stolarski, and P. K. Bhartia (2004), Implication of Version 8 TOMS and SBUV Data for Long-Term Trend Analysis, Proceedings of the Quadrennial Ozone Symposium, 1–8 June 2004, Kos, Greece, 65–66.

Geweke, J., and S. Porter-Hudak (1983), The estimation and application of long-memory time series models, *J. Time Ser. Anal.*, *4*, 221–238.

Gil-Alana, L. A. (2005), Statistical modeling of the temperatures in the Northern Hemisphere using fractional integration techniques, *J. Climate*, *18*, 5357–5369.

Granger, C. W. J. (1980), Long memory relationships and the aggregation of dynamic models, *J. Econometrics*, *14*, 227–238.

Granger, C. W. J., and R. Joyeux (1980), An introduction to long-memory time series, *J. Time Ser. Anal.*, *1*, 15–30.

Guillas, S., M. L. Stein, D. J. Wuebbles, and J. Xia (2004), Using chemistry transport modeling in statistical analysis of stratospheric ozone trends from observations, *J. Geophys. Res.*, *109*, D22303, doi:10.1029/2004JD005049.

Hadjinicolaou, P., J. A. Pyle, and N. R. P. Harris (2005), The recent turnaround in stratospheric ozone over northern middle latitudes: A dynamical modeling perspective, *Geophys. Res. Lett.*, *32*, L12821, doi:10.1029/2005GL022476.

Hosking, J. R. M. (1981), Fractional differencing, *Biometrika*, *68*, 165–176.

Hurst, H. E. (1951), Long-term storage capacity of reservoirs, *Trans. Am. Soc. Civ. Eng.*, *116*, 770–799.

Jánosi, I. M., and R. Müller (2005), Empirical mode decomposition and correlation properties of long daily ozone records, *Phys. Rev. E*, *71*, 056126, doi: 10.1103/Phys-838RevE.71.056126.

Kantelhardt, J. W., E. Koscielny-Bunde, H. H. A. Rego, S. Havlin, and A. Bunde (2001), Detecting long-range correlations with detrended fluctuation analysis, *Physica A*, *295*, 441.

Kolmogorov, A. N. (1940a), Curves in Hilbert space which are invariant with respect to one-parameter group motion, *Dokl. Akad. Nauk SSSR*, *26*, 6–9.

Kolmogorov, A. N. (1940b), Wiener's spiral and some interesting curves in Hilbert space, *Dokl. Akad. Nauk SSSR*, *26*, 115–118.

Mandelbrot, B. B., and J. W. Van Ness (1968), Fractional Brownian motions, fractional noises and applications, *SIAM Rev.*, *10*, 422–437.

Maraun, D., H. W. Rust, and J. Timmer (2004), Tempting long-memory—On the interpretation of DFA results, *Nonlinear Processes Geophys.*, *11*, 495–503.

Miller, A. J., et al. (2006), Examination of ozonesonde data for trends and trend changes incorporating solar and Arctic oscillation signals, *J. Geophys. Res.*, *111*, D13305, doi:10.1029/2005JD006684.

Moulines, E., and P. Soulier (2002), Semiparametric spectral estimation for fractional processes, In *Theory and Applications of Long-Range Dependence*, edited by P. Doukhan, G. Oppenheim, M. S. Taqqu, 251–301, Springer, New York.

Newchurch, M. J., et al. (2003), Evidence for slowdown in stratospheric ozone loss: First stage of ozone recovery, *J. Geophys. Res.*, *108*(D16), 4507, doi:10.1029/2003JD003471.

Newman, P. A., S. R. Kawa, and E. R. Nash (2004), On the size of the Antarctic ozone hole, *Geophys. Res. Lett.*, *31*, L21104, doi:10.1029/2004GL020596.

Parke, W. R. (1999), What is fractional integration?, *Rev. Econ. Stat.*, *81*, 632–638.

Pelletier, J. D. (1997), Analysis and modeling of natural variability of climate, *J. Clim.*, *10*, 1331–1342.

Randel, W. J., and J. B. Cobb (1994), Coherent variations of monthly mean total ozone and lower stratospheric temperature, *J. Geophys. Res.*, *99*, 5433–5447.

Randel, W. J., F. Wu, and R. Stolarski (2002), Changes in column ozone correlated with the stratospheric EP flux, *J. Meteorol. Soc. Jpn.*, *80*, 849–862.

Reinsel, G. C., et al. (2002), On detection of turnaround and recovery in trend for ozone, *J. Geophys. Res.*, *107*(D10), 4078, doi:10.1029/2001JD000500.

Reinsel, G. C., et al. (2005), Trend analysis of total ozone data for turnaround and dynamical contributions, *J. Geophys. Res.*, *110*, D16306, doi:10.1029/2004JD004662.

Robinson, P. M. (1995a), Log-periodogram regression of time series with long range dependence, *Ann. Stat.*, *23*, 1048–1072.

Robinson, P. M. (1995b), Gaussian estimation of long range dependence, *Ann. Stat.*, *23*, 1630–1661.

Robinson, P. M. (2005), Efficiency improvements in inference on stationary and nonstationary fractional time series, *Ann. Stat.*, *33*, 1800–1842.

Smith, R. L. (1993), Long-range dependence and global warming, In *Statistics for the Environment* edited by V. Barnett and F. Turkman, 141–161, John Wiley, Hoboken, N. J.

Smith, R. L., and F.-L. Chen (1996), Regression in long-memory time series, In *Athens Conference on Applied Probability and Time Series: Volume II. Time Series Analysis in Memory of E.J. Hannan*, edited by P. M. Robinson and M. Rosenblatt. *Springer Lecture Notes in Statistics,* 115, 378–391.

Solomon, S., R. W. Portmann, R. R. Garcia, L. W. Thomason, L. R. Poole, and M. P. McCormick (1996), The role of aerosol variations in anthropogenic ozone depletion at northern mid-latitudes, *J. Geophys. Res.*, *101*, 6713–6728.

SPARC (Stratospheric Processes and Their Role in Climate) (1998), SPARC/IOC/GAW Assessment of Trends in the Vertical Distribution of Ozone, edited by N. Harris, R. Hudson, and C. Phillips, SPARC Report No. 1, WMO Global Ozone Research and Monitoring Project Report No. 43, 289 pp., Verrieres le Buisson, France.

Stephenson, D. B., V. Pavan, and R. Bojariu (2000), Is the North Atlantic oscillation a random walk?, *Int. J. Climatol.*, *20*, 1–18.

Stolarski, R. S., et al. (1992), Measured trends in stratospheric ozone, *Science*, *17*, 342–349, doi:10.1126/science.256.5055.342.

Stolarski, R. S., and S. Frith (2006), Search for evidence of trend slowdown in the long-term TOMS/SBUV total ozone data record: The importance of instrument drift uncertainty, *Atmos. Chem. Phys.*, *6*, 4057–4065.

Stolarski, R. S., A. R. Douglass, S. Steenrod, and S. Pawson (2006), Trends in stratospheric ozone: Lessons learned from a 3D chemical transport model, *J. Atmos. Sci.*, *63*, 1028–1041.

Taqqu, M. S. (2002), Fractional Brownian motion and long-range dependence, In *Theory and Applications of Long-Range Dependence*, edited by P. Doukhan, G. Oppenheim, and M. S. Taqqu, 5–38, Springer, New York.

Toumi, R., J. Syroka, C. Barnes, and P. Lewis (2001), Robust non-Gaussian statistics and long-range correlation of total ozone, *Atmos. Sci. Lett.*, *2*, doi:10.1006/asle.2001.0042.

Tsonis, A. A., P. J. Roebber, and J. B. Elsner (1999), Long-range correlations in the extratropical atmospheric circulation: Origins and implications, *J. Clim.*, *12*, 1534–1541.

Varotsos, C., and D. Kirk-Davidoff (2006), Long-memory processes in ozone and temperature variations at the region 60°S–60°N, *Atmos. Chem. Phys.*, *6*, 4093–4100.

von Storch, H., and F. W. Zwiers (1999), *Statistical Analysis in Climate Research*, Cambridge Univ. Press, New York.

Weatherhead, E. C., and S. B. Andersen (2006), The search for signs of recovery of the ozone layer, *Nature*, *441*, doi:10.1038/nature04746.

Weatherhead, E. C., et al. (1998), Factors affecting the detection of trends: Statistical considerations and applications to environmental data, *J. Geophys. Res.*, *103*, 17,149–17,161.

Weatherhead, E. C., et al. (2000), Detecting the recovery of total column ozone, *J. Geophys. Res.*, *105*, 22,201–22,210.

Weiss, A. K., J. Staehelin, C. Appenzeller, and N. R. P. Harris (2001), Chemical and dynamical contributions to ozone profile trends of the Payerne (Switzerland) balloon soundings, *J. Geophys. Res.*, *106*, doi:10.1029/2000JD000106.

World Meteorological Organization (WMO) (1988), *Report of the International Ozone Trends Panel-1988*, Global Ozone Research and Monitoring Project, Report No. 18, Geneva, Switzerland.

World Meteorological Organization (WMO) (1999), *Scientific Assessment of Ozone Depletion: 1998*, Global Ozone Research and Monitoring Project, Report No. 44, Geneva, Switzerland.

World Meteorological Organization (WMO) (2003), *Scientific Assessment of Ozone Depletion: 2002*, Global Ozone Research and Monitoring Project, Report No. 47, Geneva, Switzerland.

Yajima, Y. (1988), On estimation of a regression model with long-memory stationary errors, *Ann. Stat.*, *16*, 791–807.

V. E. Fioletov, Environment Canada, 4905 Dufferin St., Toronto, ON M3H 5T4, Canada.

T. G. Shepherd and D. I. Vyushin, Department of Physics, University of Toronto, 60 St. George St., Toronto, Ontario M5S 1A7, Canada. (vyushin@atmosp.physics.utoronto.ca)